LEVEL

(14)

AD A100353

R and D CENTER LABORATORY

TECHNICAL REPORT

NO. 12571

U.S. ARMY TACOM

A STUDY OF MECHANICAL ALLOYING

OF METAL POWDERS

May 1981

DTIC ELECTE JUN 1 8 1981

C

by T. K. Wassel

L. Himmel

U.S. ARMY TANK-AUTOMOTIVE COMMAND
RESEARCH AND DEVELOPMENT CENTER
Warren, Michigan 48090

81 6 17 028

NOTICES

Unclassified

SECURITY CLASSIFICATION OF THIS PAGE (When Data Entered)

REPORT DOCUMENTATION PAGE		READ INSTRUCTIONS BEFORE COMPLETING FORM
1. REPORT NUMBER 12571	2. GOVT ACCESSION NO. AD-A100 353	3. RECIPIENT'S CATALOG NUMBER
4. TITLE (and Subtitle) (6) A Study of Mechanical Alloying of Metal Powders		5. TYPE OF REPORT & PERIOD COVERED (9) Final Report. Oct 77 — Sep 78
		6. PERFORMING ORG. REPORT NUMBER
7. AUTHOR(s) (10) T. K. Wassel, L. Himmel		8. CONTRACT OR GRANT NUMBER(s) (12) 95
9. PERFORMING ORGANIZATION NAME AND ADDRESS Commander, US Army Tank-Automotive Command, ATTN: DRSTA-RCKM, Warren, MI 48090 (17)		10. PROGRAM ELEMENT, PROJECT, TASK AREA & WORK UNIT NUMBERS 61101A, (16) 1T161101A91A, 00, 540EH
11. CONTROLLING OFFICE NAME AND ADDRESS Commander, US Army Tank-Automotive Command, ATTN: DRSTA-Z, Warren, MI 48090 (11)		12. REPORT DATE May 1981
		13. NUMBER OF PAGES 81
14. MONITORING AGENCY NAME & ADDRESS (if different from Controlling Office) (14) TACOM-TR-12571		15. SECURITY CLASS. (of this report) Unclassified
		15a. DECLASSIFICATION/DOWNGRADING SCHEDULE

16. DISTRIBUTION STATEMENT (of this Report)

Approved for public release, distribution unlimited

17. DISTRIBUTION STATEMENT (of the abstract entered in Block 20, if different from Report)

18. SUPPLEMENTARY NOTES

19. KEY WORDS (Continue on reverse side if necessary and identify by block number)

Mechanical alloying
ball mill
x-ray diffraction
homogeneity
metal powder

20. ABSTRACT (Continue on reverse side if necessary and identify by block number)

This investigation was undertaken primarily to obtain information concerning the chemical and structural homogeneity of mechanically alloyed powders and to determine under what conditions, if any, true solid solutions may be formed. Four different alloy systems were selected for study: 1) 50 w/o Cr - 50 w/o Mo, 2) Type 316 stainless steel, 3) 20.8 w/o Mn - 79.2 w/o Bi, and 4) a β-Ti alloy (Ti-11Cr-8Mn-5Mo-3Al).

In both the Cr-Mo system and Type 316 stainless steel system, it was

DD FORM 1 JAN 73 1473 EDITION OF 1 NOV 65 IS OBSOLETE

Unclassified

SECURITY CLASSIFICATION OF THIS PAGE (When Data Entered)

410411

established by x-ray diffraction methods that the elemental components had become interdispersed on an atomic scale as a result of high-energy milling, but that a minimum threshold speed is necessary to obtain a significant degree of alloying. However, annealing studies on the milled powders provided strong indications that the solid solutions formed by mechanical alloying are very inhomogeneous from a chemical and structural point of view.

Milling difficulties were encountered with the β-Ti and Bi-Mn powder systems which precluded any conclusions pertaining to structural or chemical homogeneity in these systems. In both the Bi-Mn and β-Ti systems, the tendency toward cold-welding and/or diffusion bonding of the particles was so pronounced that it was not possible to achieve a proper balance of cold-welding and particle fracturing in order to mechanically alloy component metals.

It was shown that the addition of oxides to the 316 stainless steel powder system retarded the rate of processing; the amount of oxide present produced significant changes in the particle size, size distribution and morphology. It was established by direct observation that the distribution of the oxide within the particles was uniform.

The effects of certain milling parameters on the rate of processing were also determined. The results confirm the conclusions of previous investigations performed by Benjamin at INCO.

TACOM FINAL REPORT NUMBER 12571

Final Technical Report

A STUDY OF MECHANICAL ALLOYING OF METAL POWDERS

BY

T. K. Wassel
(TACOM)

L. Himmel
(Wayne State University)

May 1981

US Army Tank-Automotive Command
Research and Development Center
Warren, MI 48090

TABLE OF CONTENTS

Page

FOREWORD

This final report covers work performed under In-House Laboratory Initiated Research (ILIR) at TACOM during the period October 1977 - September 1978.

The authors would like to thank Mr. D. T. Ostberg of the Tank-Automotive Research and Development Command for his assistance throughout the total program effort, and Dr. J. M. Dahl of the Climax Molybdenum Company for the preparation of the arc-cast Cr-Mo button.

ABSTRACT

This investigation was undertaken primarily to obtain information concerning the chemical and structural homogeneity of mechanically alloyed powders and to determine under what conditions, if any, true solid solutions may be formed. Four different alloy systems were selected for study: 1) 50 w/o Cr - 50 w/o Mo, 2) Type 316 stainless steel, 3) 20.8 w/o Mn - 79.2 w/o Bi, and 4) a β-Ti alloy (Ti-11Cr-8Mn-5Mo-3Al).

In both the Cr-Mo system and Type 316 stainless steel system, it was established by X-ray diffraction methods that the elemental components had become interdispersed on an atomic scale as a result of high-energy milling, but that a minimum threshold speed is necessary to obtain a significant degree of alloying. However, annealing studies on the milled powders provided strong indications that the solid solutions formed by mechanical alloying are very inhomogeneous from a chemical and structural point of view.

Milling difficulties were encountered with the β-Ti and Bi-Mn powder systems which precluded any conclusions pertaining to structural or chemical homogeneity in these systems. In both the Bi-Mn and β-Ti systems, the tendency toward cold-welding and/or diffusion bonding of the particles was so pronounced that it was not possible to achieve a proper balance of cold-welding and particle fracturing in order to mechanically alloy component metals.

It was shown that the addition of oxides to the 316 stainless steel powder system retarded the rate of processing; the amount of oxide present produced significant changes in the particle size, size distribution and morphology. It was established by direct observation that the distribution of the oxide within the particles was uniform.

The effects of certain milling parameters on the rate of processing were also determined. The results confirm the conclusions of previous investigations performed by Benjamin at INCO.

LIST OF TABLES

LIST OF FIGURES

1. INTRODUCTION

Most commercial alloys are produced by melting and casting, the components being heated together in order to form a homogeneous liquid solution which is then poured into a suitable mold and allowed to solidify. There are, however, many alloys which are difficult or virtually impossible to prepare in this manner. Included in this category are alloy systems in which the components have widely different melting points and vapor pressures (e.g., WC-Co) or systems whose components are not mutually soluble in the liquid state (e.g., oxide-dispersed metals or alloys such as ThO_2-Ni). Incongruently melting intermetallic phases (or "intermetallic compounds") are also difficult to prepare in a pure state by melting and casting since these phases often form via peritectic reactions at temperatures that are too low to permit the reaction to be completed in reasonable times. For systems of this kind, other alloying techniques such as powder metallurgy (P/M) processing must be employed. A recently developed powder processing technique known as mechanical alloying[1-3], which circumvents many of the limitations of melting and casting, and of more conventional powder processing techniques, constitutes the subject of the present report.

In conventional P/M processing, the powders are mechanically blended, usually by ball milling, and then consolidated in various ways to produce a dense, relatively fine-grained solid. The starting powders may consist of essentially pure metals, prealloyed metal powders, refractory metal oxides (or carbides, nitrides, borides, silicides, etc.) or various combinations thereof. The mechanically blended powders are consolidated by the application of heat and pressure. These operations may be performed in sequence, i.e., by cold pressing and then sintering, or simultaneously, i.e., by some form of hot working (e.g., hot isostatic pressing, hot forging, rolling or extrusion, etc.). Depending upon the chemical composition of the system, sintering of the cold pressed powders may be carried out below the solidus temperature (solid-state sintering) or above the solidus (liquid-phase sintering). Conventional powder processing methods also have their limitations, however. Problems often arise not only in achieving adequate chemical homogeneity, but especially in obtaining dispersions of second-phase particles that are fine enough and with a sufficiently uniform distribution throughout the metal matrix to impact a significant strengthening effect.

When elemental powders of two or more different metals are used as starting materials, the degree of chemical homogeneity attained in the final product depends upon how uniformly the powders have been mixed or blended, and upon the sizes (and size distributions) of the particles in the original powder mixture. Blends of coarse elemental powder particles may require prolonged high-temperature homogenization treatments, which are not only uneconomical, but can also result in undesired grain growth in the powder compact. Although the problem may be avoided by making use of prealloyed powders, this may not always be possible. Homogenization temperatures and times can also be reduced by using ultra-fine powders, i.e., powders with particle diameters less than about 10μm; however, fine metal powders are both difficult to prepare and difficult to handle. Even though such powders can be produced by the comminution of coarser powders (e.g., by ball milling), there is generally a lower limit to the size of the powder particles that can be obtained due to particle welding during milling. Lubricants can be added to prevent particle welding, but this often leads to pronounced contamination of the powders.

Another serious limitation is that extremely fine metal powders tend to be pyrophoric, i.e., they burn or ignite spontaneously in air.

The shortcomings of conventional P/M processing become even more apparent when the microstructural requirements that must be met in producing oxide dispersion-strengthened alloys are considered. In order to achieve significant strengthening effects, the particles of the dispersed oxide phase must be of the order of 100 Å to at most 1000 Å (0.01 to 0.1μm) in diameter and the mean free-path between these particles must be of the order of 0.5μm or less[4]. This requires the use of extremely fine metal powders - no more than 5μm and preferably less than 1μm in diameter - together with dispersoid particles which are at least a factor of 100 smaller than the metallic particles. Because of the considerably finer particle size of the dispersoid, and the fact that it generally has a much lower density than the metal, it is extremely difficult to obtain uniform dispersions of the two powders by mechanical blending in a conventional ball mill. Severe problems are often encountered with segregation during mixing and blending of the powders, which results in stringering of the oxide in subsequent hot working operations.

Difficulties in the production of oxide dispersion strengthened alloys by conventional powder processing have been overcome in certain systems by developing special processing technique which dispense entirely with the need for powder blending. A well-known example is SAP (sintered aluminum powder)[5]. The SAP-type alloy is prepared by ball milling pure Al to produce an oxidized flake type powder in which more than 50% of the powder particles have a thickness of ≈0.5μm or less. After cold pressing and sintering, the material is hot extruded; this causes rupturing of the thin Al_2O_3 films on the surfaces of the Al particles and produces a relatively uniform dispersion of the oxide films in the Al matrix.

The technique used in producing TD nickel (thoria-dispersed nickel) provides another example[6]. TD nickel powder is prepared by the precipitation of inorganic salts (e.g., thorium nitrate) on the surfaces of nickel powder. Low temperature decomposition of the precipitated thorium nitrate on 2-to-5μm nickel powders results in an effective dispersion of submicron ThO_2 on the powder surfaces. The powder is treated in hydrogen to reduce any NiO which may have formed, and then compacted and hot extruded.

Internal oxidation[7] (or internal nitriding[8]) is another specialized technique which has proved useful in a limited number alloy systems. The starting material is usually a dilute solid solution alloy (in the form of thin sheet, wire or powder) containing a solute element whose oxide is much more stable thermodynamically than the oxide of the base metal. Internal oxidation is carried out at an oxygen potential that is sufficiently low to prevent the formation of an external oxide scale, but still permits oxygen to diffuse into the interior of the alloy, where is combines selectively with the more reactive solute element. The net result is that finely-dispersed particles of the solute metal oxide are precipitated <u>in situ</u>. The oxidation temperature is fairly critical. If it is too high, the resulting oxide dispersion is too coarse to provide effective high-temperature strengthening; if the temperature is too low, the time for complete oxidation become prohibitively long.

During internal oxidation, the oxide particles are precipitated at a sharply-defined reaction or oxidation front. This oxidation front advances into the interior of the alloy at a rate that is determined by the rate of diffusion of oxygen in the base metal and by the initial solute content. As the oxidation front advances, however, it slows down, thus allowing more time for diffusion, and hence for growth of the oxide particles. This often leads to a substantial increase in the average size of the oxide particles with increasing depth. To minimize this effect and to keep oxidation time within reasonable bounds, the technique is generally limited to rather thin sections[9]. Internal oxidation can be applied expeditiously to alloy powders, as Grant and his co-workers [9,10] as well as others have demonstrated. With nickel-, cobalt- and iron-base alloys, powders less than about 50μm in diameter are required[9]. The technique works quite well with some alloy systems (e.g., Cu- and Ag-base alloys), but not others. For example, Al-base and Ti-base alloys cannot be internally oxidized because the oxides of these metals are far too stable thermodynamically. For this reason, internal oxidation cannot be applied to Ni-base superalloy[1] powders. Elements like Al and Ti must be present in Ni-base superalloys to provide precipitation strengthening (from the γ' phase); however, selective oxidation of these elements (which, of course, removes them from solid solution) cannot be avoided in any practical manner.

The technique of mechanical alloying redirects attention to the powder blending process and manages to overcome the shortcomings of conventional powder blending while avoiding many of the problems or difficulties associated with the use of ultra-fine metal powders. The distinguishing feature of the mechanical alloying process is the powders are blended in a special high speed mill, in which much higher energy input rates can be obtained than in a conventional ball mill. Effective interdispersion or mechanical homogenization of the starting ingredients is accomplished by a process which involves repeated cold welding and fracturing of the powder particles. Mechanical alloying has been applied successfully to the production of oxide-dispersion strengthened Ni-base alloy powders[1,11,12] and to a number of other oxide-dispersed alloy powders as well[13-15]. Its usefulness it not limited to such systems, however. Mechanical alloying has recently been used, for example, to prepare powders of the intermetallic phase Nb_3Sn, which have subsequently been employed in the manufacture multifilamentary Cu-Nb_3Sn superconducting wire[16]. The superconducting intermetallic phase Nb_3Al has also been prepared by mechanical alloying[17].

Much of the credit for developing the process of mechanical alloying must go to J.S. Benjamin and his co-workers at the International Nickel Co. (INCO). From their studies, Benjamin and his colleaques have concluded that mechanical alloying is capable of forming true solid solutions in which the individual metals are intimately dispersed on an atomic scale. However, the evidence upon which this conclusion is based is limited and is not entirely in accord with the experience of others[16]. The major objective of the present work was to obtain additional information concerning the chemical and structural homogeneity of mechanically alloyed powders which would either confirm or refute Benjamin's claim.

Before presenting a detailed outline or plan of the present investigation (Part 5), the basic features of the mechanical alloying process will first be described (Part 2) and the previous work dealing with the mechanism of mechanical alloying will be reviewed (Part 3). Some of the more practical details connected with the consolidation and thermo-mechanical processing of mechanically alloyed powders will also be given brief consideration (Part 4).

2. THE MECHANICAL ALLOYING PROCESS

In the mechanical alloying process, the powder particles are repeatedly subjected to high impact forces by milling under dry conditions in the presence of attritive elements (e.g., steel balls) which are maintained "kinetically in a highly activated state of relative motion"[3]. The type of mill generally used for this purpose consists of a water-cooled stationary tank or chamber equipped with a rotatable shaft to which a series of impellers are attached. A high energy attrition mill of this kind is illustrated schematically in Figure 1. The mill is filled with hardened steel balls to a level sufficient to bury at least some of the impeller arms so, when the shaft is rotated, the ball charge is maintained in a continual state of relative motion throughout the mill chamber. During the milling process, the metal particles are repeatedly flattened, fractured, and rewelded. Every time two steel balls collide, they trap powder particles between them. The force of impact deforms the metal particles and creates new, atomically clean surfaces. Contact between the clean surfaces results in cold welding of the particles. The heterogeneous particles that are formed by the welding together of smaller particles have a characteristic layered structure which undergoes steady refinement as milling time proceeds.

During the early stages of the process, while the metal particles are still soft, the tendency for them to weld together into larger particles predominates. As the milling process continues, however, the hardness of the particles increases due to cold working, and the ability of the particles to withstand deformation without fracturing decreases. In time, the tendency to weld and the tendency to fracture come into balance, and thereafter the size of the particles becomes constant within a narrow range. Refinement of the internal structure of the particles continues to take place after this steady-state processing stage is reached.

Surprisingly little contamination of the powder by the iron in the steel balls is experienced during milling. In the course of the grinding process, the balls become coated with a layer of the component metals, thus preventing attrition of the balls themselves.

The processing rate, or the time needed to obtain a given degree of mechanical homogenization depends upon the work hardening characteristics and initial particle sizes of the individual metal powders as well as the characteristics of the particular mill employed. As might be expected the processing rate is also strongly energy-input dependent[3]. The most significant milling parameters appear to be the milling speed and the powder-to-ball ratio. In general, the milling speed must be such that sufficient energy is imparted to the balls to reduce the powder particles to less than one-half and preferably to about 25% of the averge initial particle diameter during a single impact collision with the balls. If this condition is not satisfied, cold welding of the particles will not take place, composite particles will not be formed, and little if any inter-dispersion of the ingredients will result. The volume of the powder being milled must also be substantially less than the so-called dynamic interstitial volume between the balls. The dynamic interstitial volume, defined as the sum of the

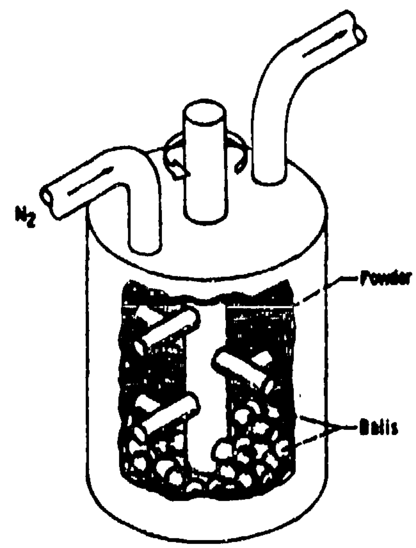

Figure 1 - High energy attrition mill (schematic).

average volumetric spaces between the balls while they are in motion, must be large enough to allow the balls to attain sufficient momentum before colliding; the volume of powder must not exceed approximately one quarter of this volume[3]. In practice, this requires that the powder-to-ball volume ratio be at most 1:12. If either of these two conditions are not satisfied, mechanical alloying will not take place to any appreciable extent.

The processing of metal powders in a high-energy mill can be contrasted with conventional ball milling. A standard ball mill consists of a rotating horizontal drum which is about half-filled with steel balls. As the drum rotates, the balls drop onto the metal powder that is being ground. The rate of grinding increases with the speed of rotation. At high speeds, however, the centrifugal force acting on the steel balls exceeds the force of gravity so that the balls are pinned to the wall of the drum, at which point the grinding action ceases. No such limitation on the energy-input rate exists in high speed attritor mills of the type previously described (Figure 1). Consequently, much higher processing rates are obtainable with such mills than with conventional ball mills.

3. THE MECHANISM OF MECHANICAL ALLOYING

In order to establish the mechanism of mechanical alloying, Benjamin and his colleaques have carried out detailed investigations on two different powder systems, one a simple binary (oxide-free) system, viz., Fe-Cr[18], the other a thoria- or yttria- dispersed, multi-component nickel-base superalloy[1]. In both cases the starting powders were processed for preselected times in a high-energy mill under a constant set of milling conditions (i.e., milling speed and powder-to-ball ratio). The Fe-Cr powders were then screen analyzed to determine the particle size distribution at various stages during milling. The powder particles from the -80, +100 size fraction were examined metallographically in order to evaluate the particle morphology and the degree of internal structural refinement which had taken place. The microhardness of selected particles from this size fraction was also measured, as was the microhardness of the layers which had welded to the surfaces of the steel balls. Only metallographic analyses appear to have been carried out on the oxide-dispersed Ni-base alloy powders. The results of these studies are summarized below.

The sequence of events which takes place during the processing of a 50 v/o Fe-50 v/o Cr powder mixture in a high speed shaker mill has been broken down into five relatively distinct time intervals: 1) an initial period; 2) a period of welding predominance; 3) a period of equiaxed particle formation; 4) the start of random welding; and 5) steady-state processing. These periods are defined in terms of: a) the powder size distribution and shape; b) the internal structure of the free powder and of the material welded to the ball surfaces; c) the hardness of the material on the ball surfaces and of the free (coarse) powders; and d) division of the material between ball surfaces and free powders.

The initial period is characterized by the devolopment of a thin welded layer (a few particles thick) on the surfaces of the balls and by the formation of both coarser and finer particles than are present in the initial powder charge (Figure 2). The material welded to the balls represents only about 1% of the total powder charge. Powder particles in the coarser fraction are platelike in shape; they are formed by flattening of the original (equiaxed) elemental powder particles. The fine powder fraction consists of both equiaxed fragments (broken off from the more friable elemental particles) and plate-shaped particles (broken off from the flattened elemental particles). The powder size distribution does not change drastically during this period and both the free powder particles and the welded layers remain relatively soft and ductile (Figure 3).

During the period of welding predominance, there is a marked increase in the relative amounts of the coarser size fractions (plate-shaped particles) while the amount of the finer fractions remains approximately constant (Figure 2). As illustrated in Figure 4a, the coarse plate-shaped powder particles now exhibit a characteristic multilayered structure. Such particles are called composite particles. The layers or lamelle within the composite particles run parallel to the major dimensions of the particles. These lamellae consist of flattened particles of the two ingredients which have welded together. The lamellar structure of the composite particles is similar to that of the material welded to the ball surfaces, indicating either that an interchange occurs between the welded layer and free powder or that the material on the ball surfaces continues

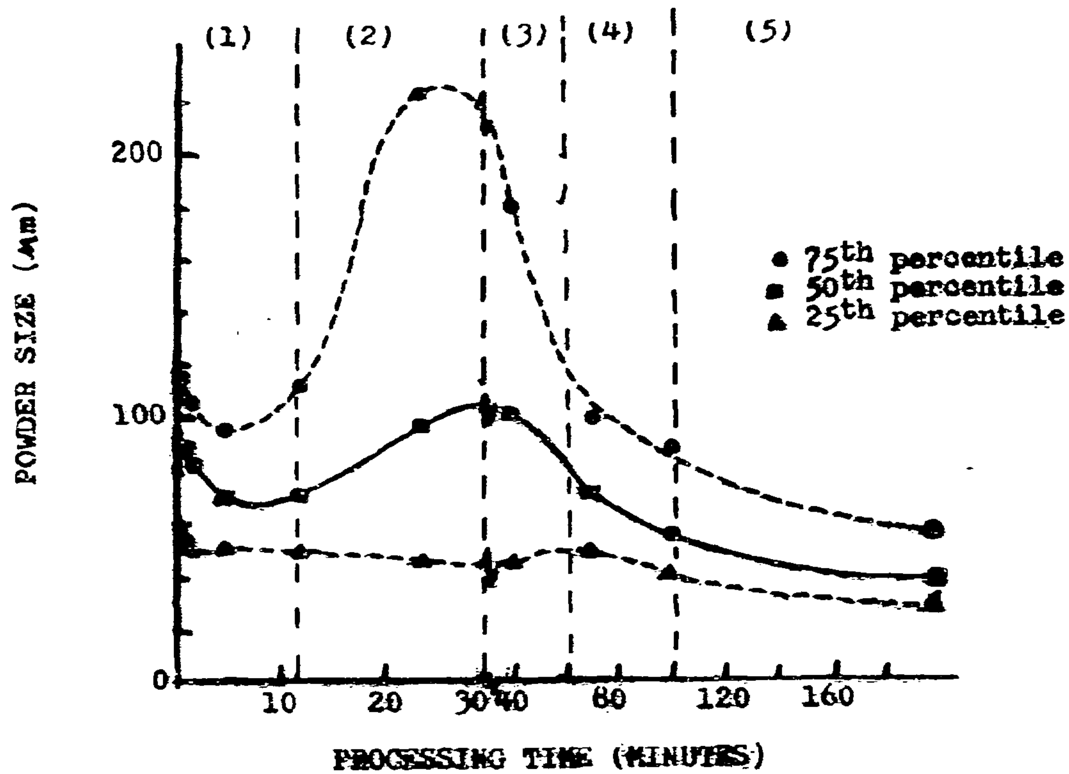

Figure 2 - Particle size distribution as a function of milling time for Fe-Cr powders processed in a high speed shaker mill. (The numbers in parentheses correspond to the five stages of processing: 1) the initial period, 2) period of welding predominance, 3) period of equiaxed particle formation, 4) start of random welding, and 5) steady state processing.) From Benjamin and Volin[18].

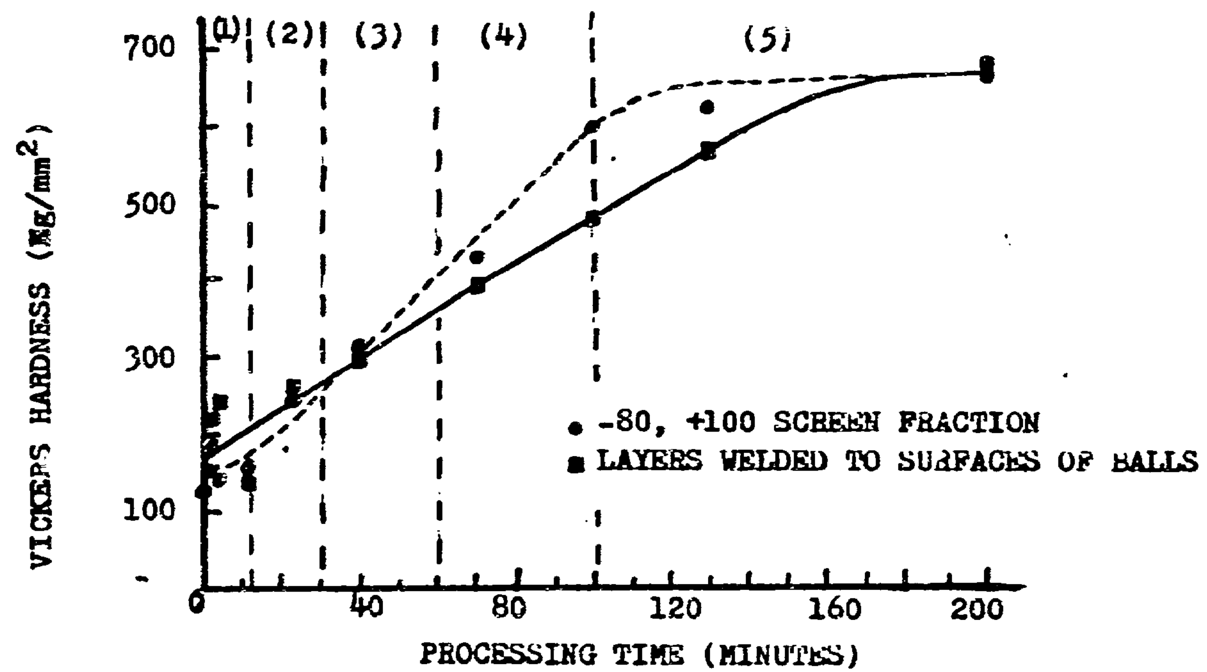

Figure 3 - Microhardness of the -80, +100 mesh powder screen fraction and of the layers welded to the surfaces of the balls as a function of processing time. (The numbers in parentheses correspond to the five stages of processing.) From Benjamin and Volin[18].

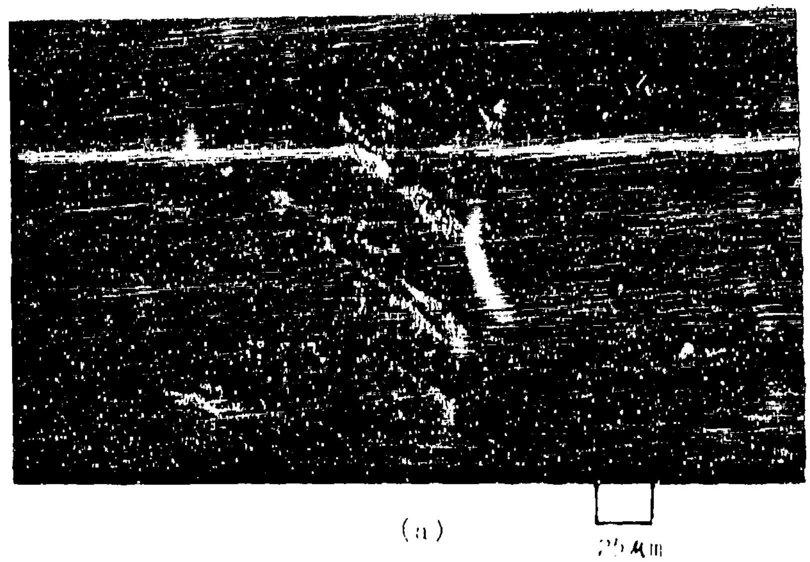

(a)

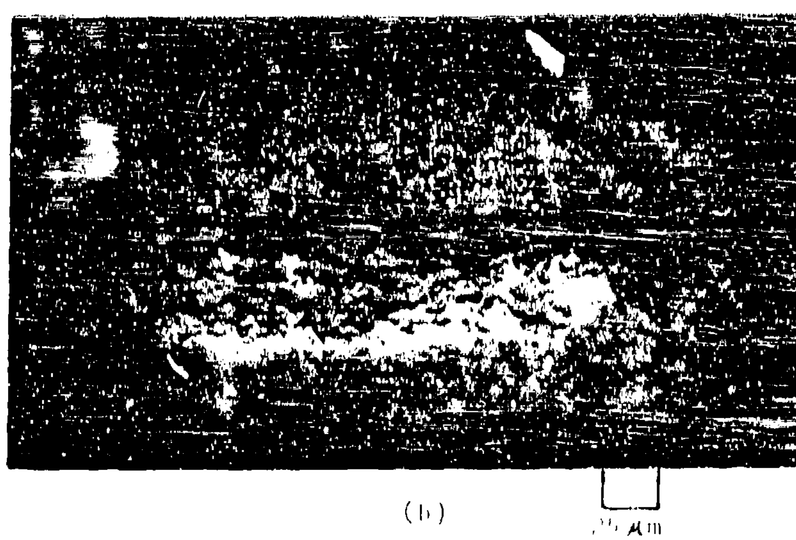

(b)

Figure 4 - Structure of -80, +100 mesh Fe-Cr powder processed in a high speed shaker mill: a) This multi-layered structure corresponds to that present in the particles during the period of welding predominance, b) This convoluted lamellar structure is observed after the start of random welding. From Benjamin and Volin[18].

to be processed at about the same rate as does the free powder. The fine particles remain elemental during this period, although they are now predominately plate-shaped. These fine particles do not possess the layered structure characteristic of the coarser composite particles; they are believed to represent pieces fractured from the edges of flattened elemental particles which did not cold weld to other particles. The hardness of the coarse powders and of the welded layers is now noticeably greater than that of the starting powders (see Figure 3).

Continued processing results in a sharp decrease in the quantity of coarse plate-shaped particles as well as the emergence of particles having more nearly equiaxed dimensions. This behavior is associated with the continued rise in the hardness of the composite particles, which has now brought about a significant decrease in their ductility. The elemental fragments virtually disappear during this period, which is also marked by the appearance of fine composite particles having a lamellar structure similar to that of the coarser particles. These fine composite particles originate from the comminution of multi-layered particles within the coarser size fraction.

The start of random welding is characterized by a pronounced change in the shape or appearance of the lamellae in both the welded layers and in the coarser powder fraction. The lamellae become convoluted instead of parallel (see Figure 4b). This convoluted shape is due to the welding together of equiaxed powder particles without any particular preference to the orientation in which they weld. This is in contrast to the behavior observed in earlier stages of the process, when the flake-like particles tend to reweld with their long axes parallel. The hardness of the powder particles continues to increase steadily during this period (see Figure 3); concurrently, a decrease in the proportion of the coarser sizes is noted as the ductility of the powder declines. The proportion of powder welded to the balls increases to approximately 6 percent during this stage. This is probably the result of the depletion of residual oxygen in the milling atmosphere (due to the adsorption on the fresh metal surfaces created during welding) which, in turn, enhances welding of the powder to the steel balls.

Still longer processing times result in a steady-state distribution of particle sizes which is dependent upon the composition of the system and the processing parameters. The product is now characterized by an increasing internal homogeneity of all the powder size fractions to a degree that can no longer be monitored by optical examination. The amount of material welded to the balls decreases to around one percent during this steady-state processing period, and the hardness of the free powders and of the welded layers both reach about the same limiting or saturation hardness (Figure 3). During this steady-state processing period, a rather delicate balance exists between the tendency for the smaller particles to weld together to form larger aggregates and the tendency of the coarser particles to fracture into smaller pieces when struck by the balls. The overall effect is to drive both groups of particles toward the middle of the size range and therefore to produce a relatively narrow (and constant) size distribution.

The rate of internal structural refinement of the coarse composite particles was determined by measuring the average lamellar thickness of these particles as a function of processing time. Particles from the -80, +100 mesh size fraction were selected for the measurements because these particles are larger than any of those in the original powder mixture and therefore must have been acted upon (at least once) by the balls. The data obtained are plotted in Figure 5. Note that the average lamellar thickness is about twice the spacing between welds because, statistically, welds between similar constituents (i.e., Fe/Fe and Cr/Cr welds) are formed about as often as those between Fe and Cr. Except during the initial period, it is found that, to a first approximation, the average lamellar thickness decreases exponentially with processing time. Unfortunately, however, the measurements shown in Figure 5 could not be extended into the steady-state processing period due to limitations on the resolution of the optics. Well before the steady-state processing stage is reached, the average lamellar spacing is reduced to below about 0.9μm ($\approx$9000 Å), which is the limit of resolution obtainable with the optics Benjamin employed.

It is safe to assume that structural refinement of the composite particles continues beyond the stage where the lamellae can no longer be resolved optically. However, whether, with further processing, the composite particles still consist of discrete fragments of decreasing size, or true solid solutions are eventually formed, cannot be decided on the basis of these measurements alone. An extrapolation of the data by nearly four orders of magnitude would be required before interdispersion of the two components on an atomic scale could be inferred. A linear extrapolation of the data in Figure 5 over so broad a range is unwarranted, especially since there are indications[2] the rate of structural refinement may actually fall off slightly during the steady-state processing stage due to the extremely high hardness (accumulation of strain energy) which the particles have now acquired.

The evidence that true solid solutions may be formed in certain systems as a result of high-energy milling is largely of an indirect nature and can hardly be considered conclusive. It has been found, for example, when elemental Ni and Cr powders are processed in a high-energy mill, the magnetic response of the milled powder (Ni is ferromagnetic, Cr is not) decreases rapidly even during the early stages. By the time the individual lamellae within the composite particles could no longer be resolved optically, the magnetic response reached a value as low as that of a completely homogenous wrought Ni-Cr alloy prepared by melting and casting. According to Benjamin[2], this shows the two metals are now intimately mixed on an atomic scale and a true solid solution had formed rather than a finely-dispersed mechanical mixture. This interpretation is questionable, however. It should also be noted that in their work on the preparation of Nb_3Sn by mechanical alloying, White and Nix[16] showed conclusively, using X-ray diffraction techniques, that, although the individual phases could not be resolved optically, their milled powders consisted of an intimate mechanical mixture of the two elemental components. It was necessary to vacuum anneal these powders in the range from 650°-850°C in order to transform the mechanical mixture to the intermetallic phase Nb_3Sn.

Another system which Benjamin has investigated in some detail involves oxide-dispersed Ni-base superalloy powders[1]. The starting ingredients consisted of elemental Ni and Cr powders, a vacuum melted Ni-Al-Ti master alloy powder and either ThO_2 or Y_2O_3 in the form of loosely-agglomerated particles 100-500Å in diameter. Approximately 2.5 volume percent of ThO_2 or Y_2O_3 was added. The

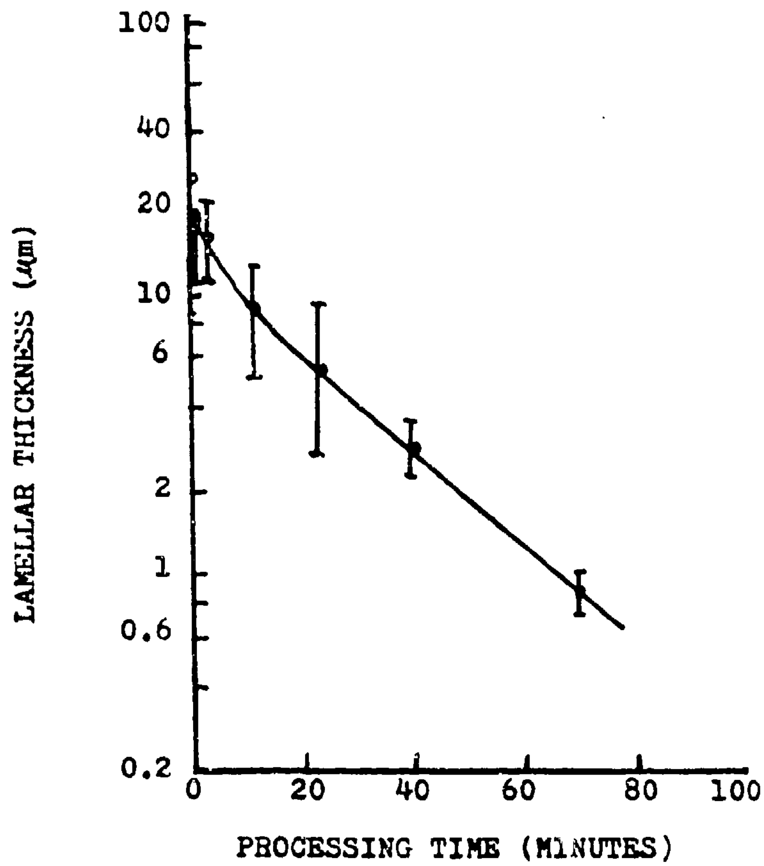

Figure 5 - Variation of lamellar thickness with processing time for Fe-Cr powders processed in a shaker mill. The measurements were made on composite particles from the -80, +100 mesh size fraction. From Benjamin and Volin[18].

powders were processed in a high-energy attritor mill of the type previously described*. A processing trend qualitatively similar to that observed in the Fe-Cr system was noted. For example, composite particles were formed at a relatively early stage, many of these particles being larger than the coarsest particles in the original powder mixture. Since nickel is the softest constituent in the starting mixture, it becomes the matrix in which the harder or more friable constituents are dispersed when composite particles are formed by cold welding. The thorium oxide or yttrium oxide disperses along welds in the composite particles.

After only a few hours of milling, unprocessed particles of the major constituents (Cr and the Ni-Al-Ti master alloy) and composite particles consisting of unprocessed fragments as well as processed fragments could be identified (Figure 6). The ThO_2 or Y_2O_3 particles could not be resolved optically, however. As time proceeds, the striated or lamellar nature of the composite particles (as delineated by the flattened Cr platelets) becomes more apparent, but the internal structure also becomes more uniform, and the proporption of unprocessed powder decreases. Both the spacing and the size of the chromium fragments within the composite particles are steadily reduced as processing continues. After about 20 hours of processing, no large Cr fragments are found within the composite particles, and the structures of both large and small composite particles are now quite similar. With still further processing, an increasing proportion of the Cr fragments within these particles are reduced in size below the limit of resolution of the optical microscope. Powders processed 40 hours or longer, therefore, appear featureless. Even though the internal structure of the composite particles can now no longer be resolved, it is likely that structural refinement continues with additional processing.

The disposition of the ThO_2 or Y_2O_3 particles during milling can only be surmised since the oxide particles are too small to be resolved optically. According to Benjamin[1,2], the thoria or yttria particles are dispersed along the welds in the composite particles. At first the welds are far apart and the concentration of oxide particles trapped at each weld is rather high. With further processing, the spacing between the welds decreases, but the spacing between oxide particles along the welds increases. Finally, when the powder has been processed to the point where the fine structure within the composite particles can no longer be resolved, i.e., when the spacing between welds has been reduced to 0.5μm or less, the mean free path between oxide particles along the welds is also of this same order, viz., about 0.5μm. Benjamin states that this nearly uniform dispersion of the oxide particles in the metal matrix cannot be enhanced by further processing, but the basis for this statement is not mentioned. These thoriated or yttriated Ni-base superalloy powders were subsequently consolidated by hot extrusion (see Part 4). Electron micrographs (replica technique) of the consolidated alloys showed that the oxide particles were indeed uniformly distributed throughout the matrix and that these particles were all considerably less that 1000Å ($<0.1\mu$m) in diameter.

---

*A mill of exactly the same design has been used in the present investigation. Refer to Part 6 for a more complete description.

Figure 6 - Structure of composite Ni-Cr-(Ni-Al-Ti) master alloy powders processed in a 10-S Attritor mill (132 RPM). This corresponds to the structure present in the particles during the initial period of processing (X285). From Benjamin[1].

4. CONSOLIDATION AND THERMO-MECHANICAL PROCESSING OF MECHANICALLY-ALLOYED POWDERS

Mechanically-alloyed powders are most often consolidated by hot working (i.e., hot extrusion) rather than by cold compaction and sintering. There are a number of reasons for this. Since mechanically-alloyed powders are heavily cold worked and have a somewhat narrow size distribution, cold pressing would not be expected to yield compacts having a very high green density or green strength. Relatively high sintering temperatures (and/or long sintering times) would therefore be needed to obtain densification, thus negating any advantage that the initial chemical homogeneity of the mechanically-alloyed powders might otherwise have conferred. In the case of oxide-dispersed powders, the high sintering temperatures required for densification may also result in unwanted coarsening of the oxide distribution.

An even more compelling reason for hot working is in order to achieve good high-temperature strength, it is necessary to develop a fibrous microstructure consisting of elongated grains with a high aspect ratio (i.e., high length-to-diameter ratio). This can be accomplished by hot extrusion (and/or hot rolling), but not by cold pressing and sintering alone. A practical process[19] for the manufacture of oxide dispersion-strengthened Ni-base superalloys is illustrated schematically in Figure 7. The mechanically-alloyed powder is sealed in an evacuated metal can and then hot extruded. This is followed by hot rolling and gradient annealing, which produces the high grain aspect ratio that is so essential for good high-temperature strength.

The ThO_2- and Y_2O_3- dispersed Ni-base superalloy powders which Benjamin prepared[1] were consolidated by hot extrusion at about 1180°C at a 12:1 extrusion ratio. Elongated grains running parallel to the extrusion axis were produced by a simple homogenization and grain coarsening anneal (2 hours at 1275°C). Subsequently, the alloys were given a solution heat treatment (7 hours at 1080°C), air cooled and then aged for 16 hours at 705°C in order to precipitate the γ'-phase*. The metal matrices in these thoriated and yttriated alloys are quite similar in composition to Nimonic 80A, a commercially-available Ni-base superalloy produced by the International Nickel Co., Inc. The stress-rupture properties of these oxide dispersion-strengthened alloys were therefore determined and compared with stress-rupture data for Nimonic 80A as well as for TD nickel.

Some of the stress rupture data are reproduced in Figure 8, in which the rupture stresses for 1000 hour life are plotted as a function of the temperature for all

---

*This is a fairly conventional heat treatment for Ni-base superalloys. The precipitation of fine γ' [$Ni_3(Al,Ti)$] in the γ(fcc) matrix is required for intermediate temperature strengthening. Independent studies have shown, for example, that the intermediate temperature rupture life is controlled by the amount of fine γ'($\leq$0.2μm) that is present[11]; high rupture strengths or rupture lives are obtained by maximizing the amount of fine γ' through proper adjustment of the chemical composition and appropriate heat treatment.

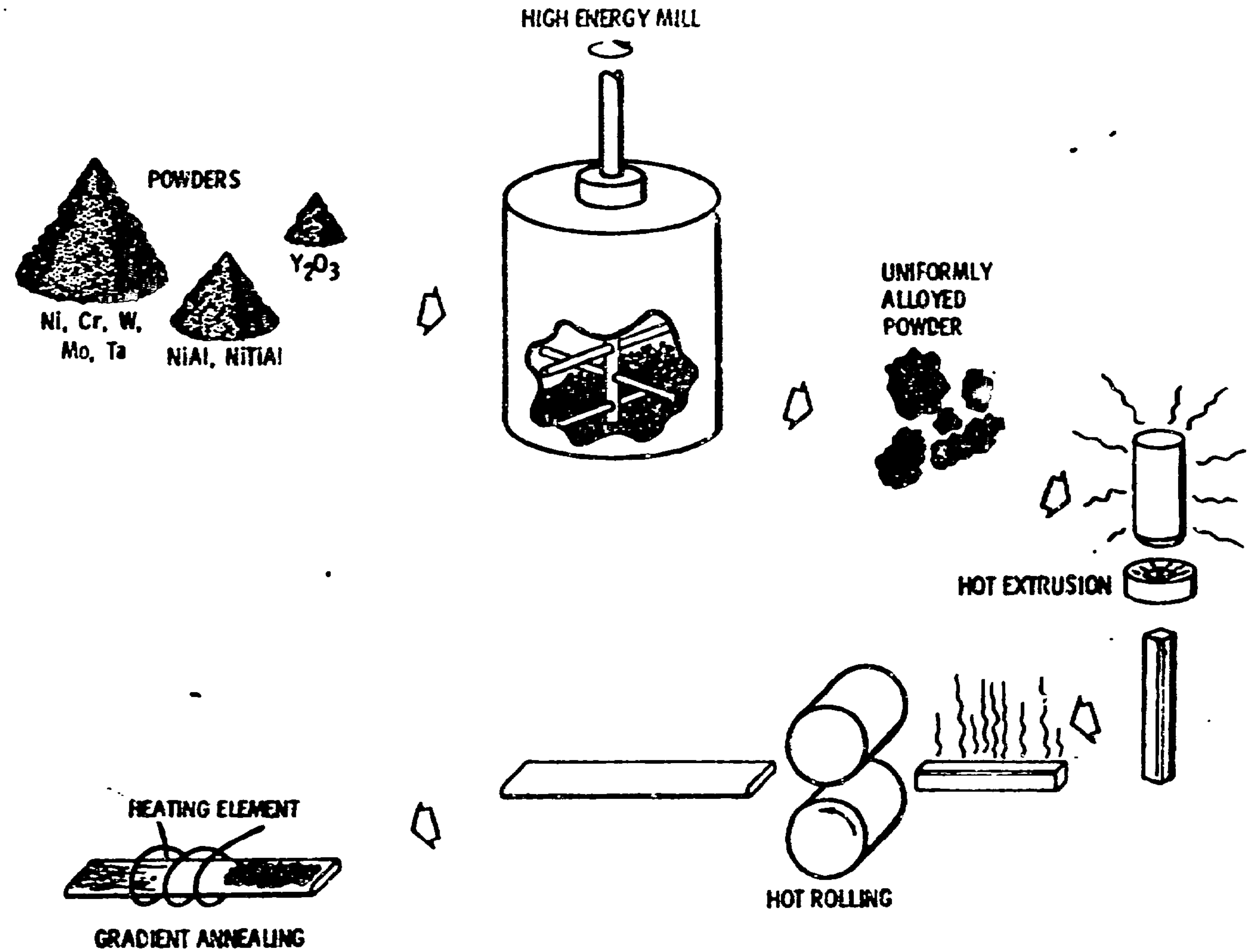

Figure 7 - Process for manufacture of an oxide dispersion strengthened superalloy. From Glaskow[19].

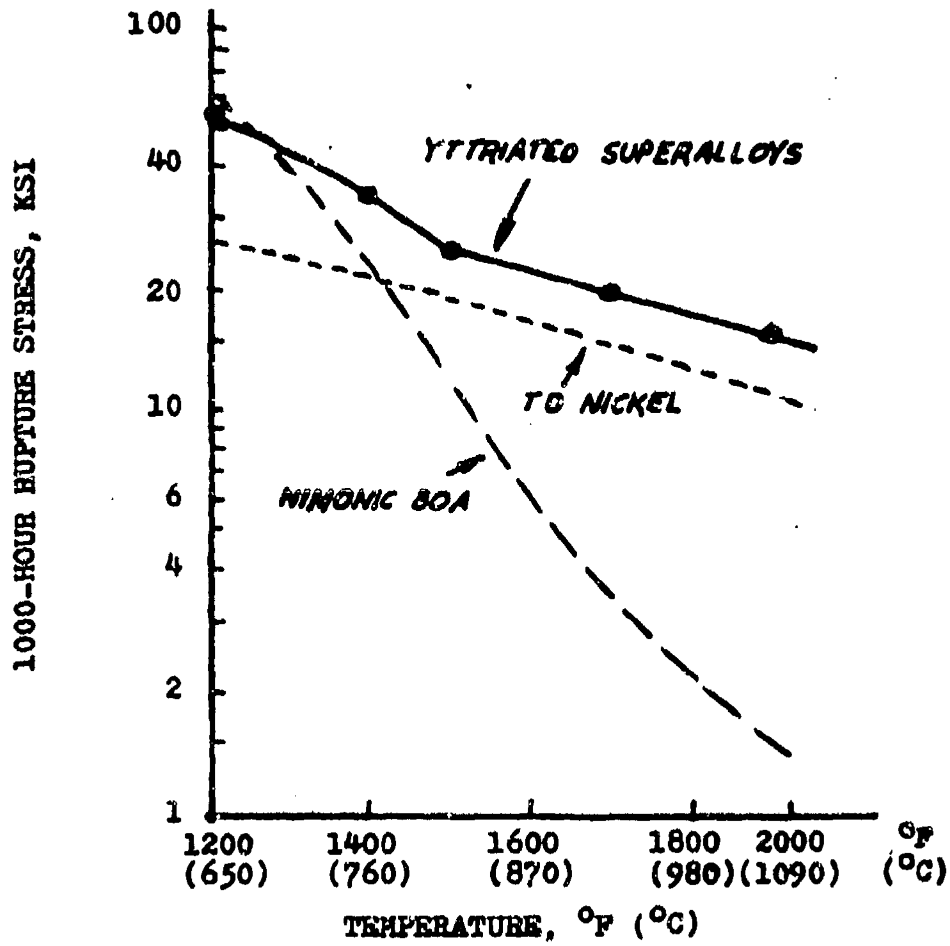

Figure 8 - Comparison of the rupture stress for 1000 hour life in yttriated Ni-base superalloys with similar data for Nimonic 80A and TD nickel. From Benjamin[1].

three materials. As may be seen from Figure 8, the rupture strength of the yttriated Ni-base alloys prepared from mechanically-alloyed powders is comparable to or greater than that of Nimonic 80A in the temperature range from about 700°C to 815°C (1300°F-1500°F) and far exceeds that of Nimonic 80A at higher temperatures, i.e., at temperature between about 815°C and 1040°C (1500°F-1900°F). It is also clear that more than one strengthening mechanism is operating in the yttriated Ni-base alloys. In the lower temperature range, precipitation strengthening by fine γ' is dominant, whereas oxide-dispersion strengthening predominates at higher temperatures. These two strengthening mechanisms appear to augment each other in the yttriated alloys at intermediate temperatures. Benjamin also showed that yttria is as suitable or as effective a dispersoid in Ni-base alloys as thoria. The stress-rupture properties of the yttriated alloys appeared to be somewhat superior to those of the thoriated alloys, however, this is believed to be due to differences in processing rather than to differences in the identity of the dispersoid itself.

Merrick et al.[11] have also developed an oxide dispersion-strengthened Ni-base turbine blade alloy by consolidating mechanically-alloyed powders. This alloy, designated MA 6000E, has the nominal composition 15Cr-2Mo-2Ta-4W-4.5Al-2.5Ti-0.15Zr-0.05-0.01B-1.1Y_2O_3-balance Ni. The mechanically-alloyed powders were canned, extruded at 815°C (20:1 extrusion ratio) and gradient annealed to obtain the required high grain aspect ratio. The consolidated material was then solution treated for 1/2 hour at 1230°C and air cooled to bring out the full potential of the γ' phase for intermediate temperature strengthening. The elevated temperature stress-rupture properties (1000-hour rupture stress) of MA 6000E are shown in Figure 9, along with corresponding data for a directionally-solidified Ni-base turbine alloy, Mar-M 200+Hf*, and for TD nickel.[19]

There are obvious similarities between these data and the results previously obtained by Benjamin (Figure 8). In the lower temperature range, for example, the rupture strength of the oxide-dispersed alloy MA 6000E, is comparable to that of directionally-solidified Mar-M 200, but MA 6000E displays a definite superiority at temperatures above about 900°C. At least three strengthening contributions can be identified in MA 6000E, namely, enhanced solid solution strengthening (compared, for example, to Nimonic 80A), precipitation strengthening from γ', and strengthening due to the presence of the dispersed oxide phase. As before, precipitation strengthening (together with solid solution strengthening) is dominant at lower temperatures, whereas oxide dispersion strengthening is dominant at higher temperatures.

The low cycle, elevated temperature fatigue properties of MA 6000E were also found to be superior to those of either directionally-solidified or conventionally cast Mar-M 200, as is shown in Figure 10. This has been attributed[19], in part, to the orientation of the grain boundaries, which are perpendicular to the direction

---

*The composition of Mar-M 200 is nominally 8Cr-10Co-12.5W-5Al-2Ti-1.8Nb-0.05Zr, 0.15C-0.015B-balance Ni. The addition of 1-2% Hf improves the castability of the alloy and reduces problems with hot shortness.

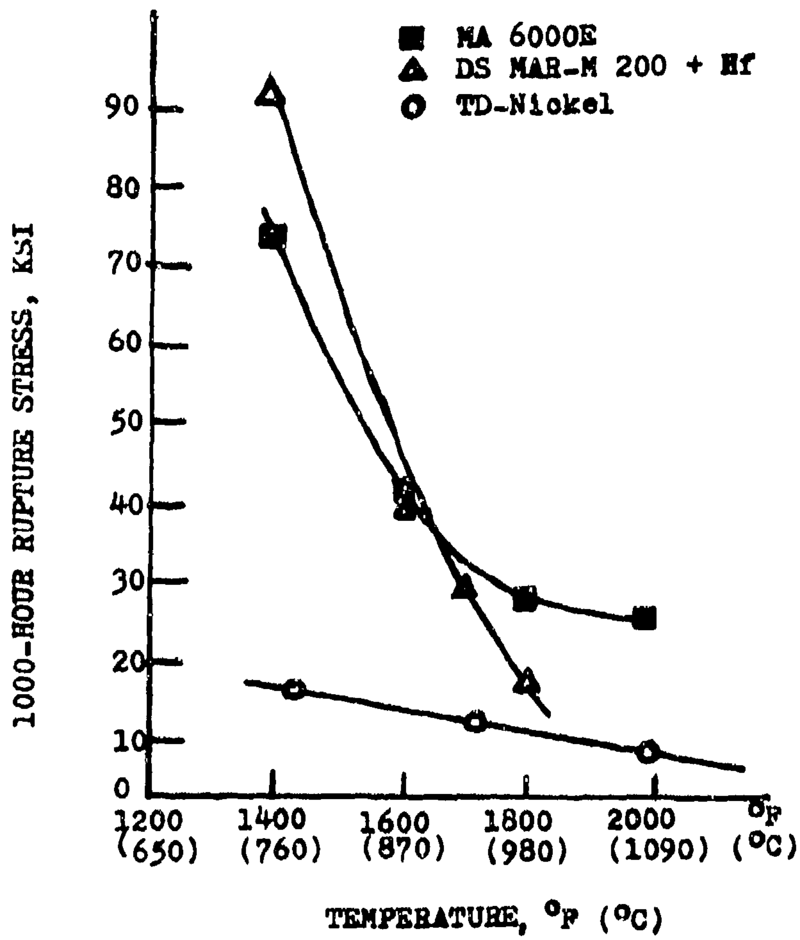

Figure 9 - Comparison of 1000 hour rupture strength of MA 6000E with directionally solidified Mar-M 200 + Hf and with TD-nickel. From Glaskow[19].

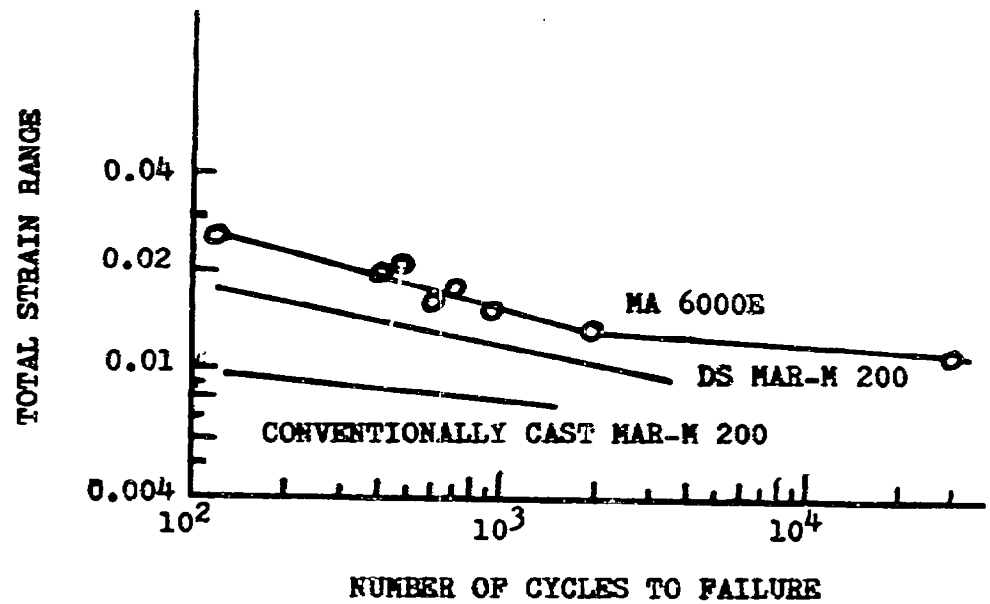

Figure 10 - Low cycle strain controlled fully reversed fatigue behavior of MA 6000E at 760°C compared with directionally solidified and conventionally cast Mar-M 200. From Glaskow[19].

of crack propogation, and, in part to the uniform dispersion of fine oxide particles. The fine oxide dispersion tends to distribute slip in the matrix more homogeneously and therefore reduces the tendency for cleavage-type cracking caused by high local stress concentrations associated with intense slip bands. Oxides, carbides or other hard phases in sizes larger than about 1μm appear to be completely absent in MA 6000E. This also has a beneficial effect. Premature crack initiation at large hard particles, which is the dominant mode of failure during high cycle fatigue in conventionally processed superalloys, is thereby avoided.

Attempts have also been made to produce an oxide dispersion strengthened Ti-base alloy by hot extrusion of mechanically-alloyed powders[13]. The matrix composition (Ti-36 w/o Al) corresponded to that of the intermetallic γ phase (TiAl, ordered fct) in the Ti-Al system; Y_2O_3 in amounts of 1.5 or 3.0 v/o were added. Difficulties were encountered both in the preparation of the mechanically-alloyed powders and during hot extrusion. The major problem in milling was that the powder tended to agglomerate and adhere to the walls of the container, which meant little free powder was obtained on discharge. Agglomeration of the powder was believed to be enhanced by diffusion bonding due to the heating up of the charge during milling. To help alleviate this problem, interrupted milling cycles were employed. The powders were milled for only relatively short periods (3 to 9 hours) and the mill contents were allowed to cool down before further processing. The resulting powders were extruded at 1410°C at a 15:1 extrusion ratio. The oxide-dispersed powders proved particularly difficult to extrude and sections of the extruded rods were often found to contain transverse cracks. Nevertheless, the tensile strengths of the oxide-dispersed alloys were found to be significantly higher than that of yttria-free TiAl both at room temperature and at temperatures up to 900°C.

In order to obtain specimens for oxidation studies, Stringer and co-workers have prepared oxide-dispersed Ni-Cr[14] and Co-Cr[15] powders by mechanical alloying. These powders were first annealed (1 hour at 1100°C in hydrogen) and subsequently consolidated by cold compaction, sintering* (55 hours at 1200°C in hydrogen), hot pressing and finally hot rolling. Non-uniform distributions of the oxide dispersoid (Y_2O_3 or CeO_2) were obtained in the final product. Dispersoid free regions were present, but these regions are attributed to the use of consumable Ni balls in the attritor mill.

*A density only about 70% of theoretical was achieved after cold compaction and sintering. This low density resulted in edge cracking during rolling and, thus, the preceding hot pressing step was introduced to eliminate this problem.

5. OUTLINE OF THE PRESENT INVESTIGATION

As previously noted, little evidence of a direct nature currently exists to support Benjamin's contention that high-energy milling is capable of interdispersing the components of an alloy system on essentially an atomic scale. The experiments described herein were therefore designed to determine under what conditions, if any, true solid solutions may be formed as a result of mechanical alloying. X-ray powder diffraction methods have been used extensively in order to establish whether the high-energy milled powders can legitimately be regarded as solid solutions or whether they consist merely of intimate mechanical mixtures of the starting ingredients. For this purpose, diffractometer scans obtained on the milled powders were compared with diffraction spectra from the original powder mixture and from chemically homogeneous, single-phase reference standards. In two of the systems chosen for study (Cr-Mo and Type 316 stainless steel), the progress of mechanical alloying, i.e., the rate of processing, was monitored by observing the changes in peak and integrated intensities, peak positions and peak breadths for several of the most prominent Bragg reflections as a function of the processing time. Useful information concerning the structural and chemical homogeneity of the heavily cold-worked powders was also obtained from subsequent annealing experiments.

Supplementary techniques of various kinds, such as optical and scanning electron microscopy (SEM), were used to evaluate the shape or morphology of the powder particles, as well as their size and size distribution. The SEM at our disposal was also equipped with an energy-dispersive X-ray analysis (EDAX) unit and attempts were made to use this feature of the instrument to determine the spatial distribution of the component elements within individual powder particles. Unfortunately, however, the best possible X-ray resolution that could be achieved with the EDAX unit was about 1μm*. The X-ray images that were obtained could not be relied upon, therefore, to provide much more information than could be gotten by optical microscopy. In principle, energy-dispersive X-ray analysis could also have been used to obtain quantitative chemical analyses of individual powder particles. Although such measurements would undoubtedly have been of great value, they were not attempted for at least two reasons. Not only would a considerable amount of time and labor have been required in order to prepare a suitable set of standards, but, because a data acquisition and data processing system was lacking, the effort needed to collect a statistically-significant amount of data, even on a single sample, would have been prohibitive.

Four different alloy systems were selected for the present study, namely:

1.) 50 w/o Cr - 50 w/o Mo (64.8 a/o Cr - 35.2 a/o Mo)

2.) Type 316 stainless steel (Fe-17Cr-12Ni-3Mo-2Mn-1Si)

3.) 20.8 w/o Mn-79.2 w/o Bi (50 a/o Mn-50 a/o Bi)

4.) A β-Ti alloy (Ti-11Cr-8Mn-5Mo-3Al)

---

*Probably closer to 10μm in routine use.

As will become evident, greatest attention has been given to the Cr-Mo and Type 316 stainless steel systems. In general, the systems and compositions listed above were chosen for specific reasons, not the least of which was to prevent possible difficulties or ambiguities in the analysis and interpretation of the X-ray diffraction spectra beyond those unavoidably introduced by the heavily cold worked nature of the powder particles.

The Cr-Mo system, for example, is isomorphous. Both pure elements have the bcc structure and, at least at high temperatures (see Figure 11), they form a complete series of solid solutions. However, the lattice parameters for Cr (a=2.884Å) and Mo (a=3.147Å), and hence their d-spacings, are substantially different. The corresponding Bragg peaks for these two elements are therefore widely separated; the Bragg angles for the respective (110) reflections differ, in fact, by about 6.4° 2θ (see Table I and Figure 12). Since shifts in the positions of the Bragg peaks due to changes in chemical composition can easily be measured to within $\pm 0.05^\circ$ 2θ, compositional changes as small as ± 1% are readily detectable*. If a reasonably homogeneous solid solution is formed by high energy milling a 50:50 w/o mixture of the elemental components, the (110) Bragg reflections for Cr and Mo would each be shifted by roughly 3° 2θ (see Figure 12). Shifts of this magnitude should be unmistakeable, even if the Bragg peaks are severely broaded due to non-uniform strain or to compositional inhomogeneities. It should therefore be possible to determine, unambiguously, whether the milled powders consist of a mechanical mixture of the elemental components or whether solid solutions are present.

A possible complication may nevertheless arise in this system, as can be seen from the phase diagram in Figure 11. According to this diagram[21], a miscibility gap exists in the Cr-Mo system at low temperatures. This miscibility gap was calculated by Hultgren et al.[22] from high-temperature thermodynamic data. If solid solutions are indeed formed by mechanical alloying, these solutions must be metastable at room temperature, assuming that the phase diagram is correct.

The remaining three systems selected for study here are all non-isomorphous systems. The rationale behind their selection is as follows: In all three systems, the end result of mechanical alloying, assuming that the starting ingredients are intimately mixed on an atomic scale, should be a structurally homogeneous solid solution or intermetallic phase which has a crystal structure different from that of the major component of the original powder mixture. Consequently, this phase should be easily recognizable and distinguishable from the original powder mixture by X-ray diffraction analysis even if it is not chemically homogeneous. In the Type 316 stainless steel system, for example, the major component of the starting powder mixture is α-Fe, which is bcc, whereas the alloy solid solution is fcc. In the β-Ti alloy system, the major component (Ti) is hcp, but the alloy solid

---

*Lattice-parameter vs. composition data for the Cr-Mo system have been taken from a compilation by Pearson[20]. These data (Table I) have been used to calculate the Bragg angle for the (110) reflection as a function of composition. The resulting values are plotted in Figure 12.

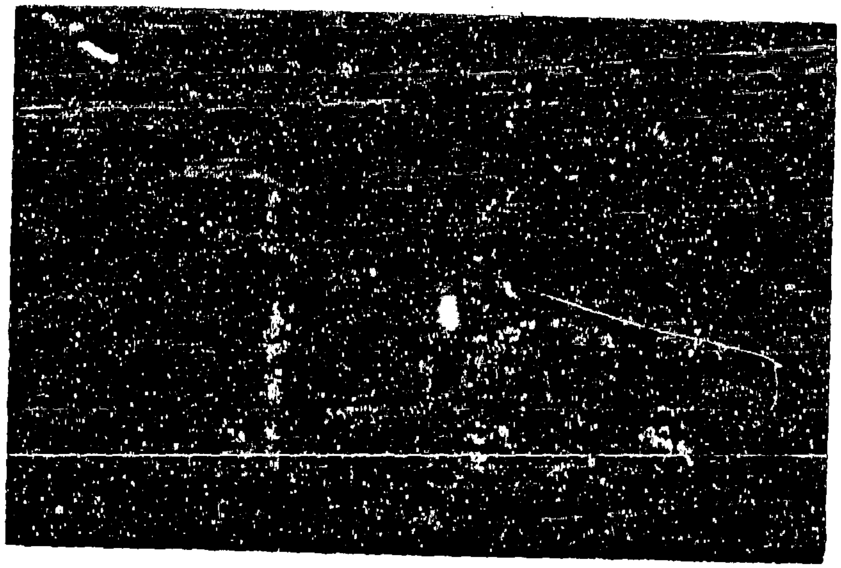

Figure 11 - Phase diagram for the Chromium-Molybdenum system[21]. Note the presence of the miscibility gap at low temperatures .

TABLE 1

LATTICE PARAMETER VS COMPOSITION DATA FOR THE Cr-Mo SYSTEM[20]
TOGETHER WITH CALCULATED d-SPACINGS AND BRAGG ANGLES FOR THE (110) REFLECTION

Data of Trzebiatowski et al.

Percentage Mo				
a/o	w/o	a, Å	d_{110}	2θ
0	0.0	2.884	2.039	68.3
10	17.0	2.921	2.065	67.3
20	31.5	2.953	2.088	66.5
30	44.1	2.982	2.108	65.8
40	55.4	3.012	2.130	65.1
50	64.8	3.039	2.149	64.4
60	73.4	3.065	2.167	63.8
70	81.1	3.092	2.186	63.2
80	88.1	3.112	2.200	62.7
90	94.3	3.132	2.215	62.2
100	100.0	3.150	2.227	61.9

Data of Kubaschewski and Schneider

0	0.0	2.884	2.039	68.3
6	10.5	2.895	2.047	68.0
12	20.1	2.924	2.067	67.3
21	32.9	2.949	2.085	66.6
26	39.3	2.968	2.099	66.1
35	49.8	2.998	2.120	65.4
45	60.1	3.032	2.144	64.4
56	70.1	3.060	2.164	63.9
66	78.2	3.087	2.183	63.3
75	84.7	3.103	2.194	62.9
84	90.6	3.116	2.203	62.6
100	100.0	3.147	2.225	61.9

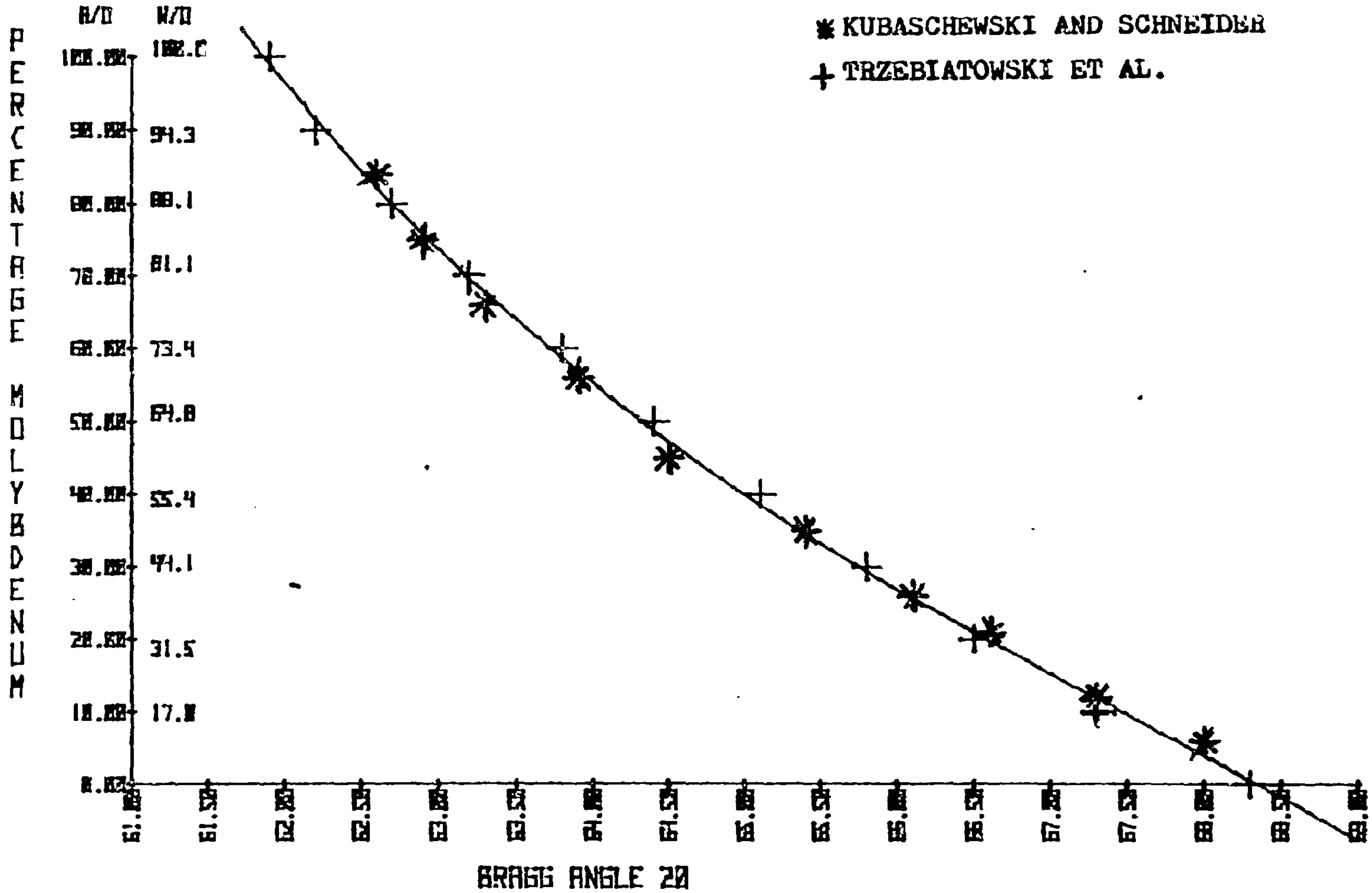

Figure 12 - Calculated Bragg angle (2θ) vs composition fcr the (110) reflection from homogeneous Cr-Mo solid solutions.

solution is bcc, at least at elevated temperatures*. The two elemental components in the Mn-Bi system have complex cubic (α-Mn) and rhombohedral (Bi) structures whereas the intermetallic phase MnBi exhibits the hexagonal nickel arsenide structure. Another reason for selecting the Mn-Bi system is that MnBi has reportedly been prepared by conventional ball milling followed by low-temperature annealing[24].

Pronounced changes in magnetic properties should also take place in both the Type 316 stainless steel and the Mn-Bi systems if structural transformations are induced by high energy milling. This provides an opportunity to monitor the progress of mechanical alloying by measuring the magnetization as a function of the milling time. In the stainless steel system, for example, the original powder mixture is ferromagnetic (due to the presence of α-Fe and Ni) but the homogeneous fcc solid solution is paramagnetic. Neither Mn or Bi are magnetic, but the intermetallic phase MnBi is strongly ferrimagnetic. Regretably, we were not able to carry out such magnetization measurements for lack of the necessary equipment and time. Some simple qualitative evaluations of the magnetic responses were made, however, particularly on the stainless steel powder mixtures.

The approach outlined above provided the major thrust of this investigation. Pertinent experimental details are given in Part 6 which follows. The results obtained and their analysis or interpretation are presented in Part 7. A number of related experiments have also been carried out, some merely to confirm previously established features of the mechanical alloying process and some of a more exploratory nature. These experiments are also described in Part 7.

---

*The Ti-13V-11Cr-3Al alloy contains relatively large amounts of β- stabilizing elements and only relatively small amounts of α- stabilizing elements. The alloy is classified as a β-phase alloy since the structure is bcc at room temperature after slow cooling from above the β-transus temperature (i.e., from above about 650°C). However, the β-phase does not appear to be thermodynamically stable at room temperature[23].

6. MATERIALS, EQUIPMENT AND EXPERIMENTAL PROCEDURES

6-1 MATERIALS AND STANDARDS

The starting metal powders used in this investigation were all elemental powders; no master alloy powders were employed. The majority of these powders were prepared by atomization, and all of them, with the exception of iron, were of relatively high purity. The sources and pertinent characteristics of these powders are listed in Table II. Small quantities (up to 3 w/o) of rutile, TiO_2, were added to the starting elemental powder mixtures in order to prepare oxide-dispersed powders and to study the effects of oxide additions on the rate of processing.

Chemically homogeneous, single-phase reference standards were needed against which the X-ray diffraction spectra for the milled powders could be compared, both before and after the powders were annealed. The reference standard used for the Cr-Mo system was a small arc-cast button prepared from a mechanically blended mixture of the elemental powders. A 50:50 w/o mixture of the blended powders was pressed into the form of a pellet which was then arc-melted using a non-consumable electrode technique. To insure good macroscopic homogeneity, the button was remelted three times, turning it top-to-bottom between each melting operation. Finally, the alloy was given a 10 hour homogenization anneal in hydrogen at 1500°C and then water quenched to avoid possible phase separation on cooling. The button was not analyzed chemically. From the measured positions of the Bragg peaks and published lattice parameter - composition data for the Cr-Mo system[20], however, it was established that the composition near the center of the button was indeed very close to 50 w/o Cr - 50 w/o Mo.

The diffraction standard used for the Type 316 stainless steel system was a pre-alloyed powder prepared by the atomization process. Since difficulties were encountered in processing the β-Ti and Mn-Bi powder mixtures, and since there was little evidence that mechanical alloying had occured in either case, no standards were prepared for these systems.

6-2 EQUIPMENT

The powders examined were processed in a laboratory Model 1-S Szegvari Attritor Grinding Mill (of the type used in ink and paint manufacture) shown schematically in Figure 1. The 1-S Attritor is a high energy ball mill of 1½ gallon capacity. The charge of low carbon steel balls (≈4mm diameter) and metal powder is held in a stationary (vertical) water-cooled, gas-tight stainless steel container and is agitated by impellers radiating from a variable speed shaft (maximum 2 horsepower @ 300 RPM). Powder is removed from the mill via a bottom discharge valve. This high energy ball mill can achieve energy input rates more than 10 times those obtainable in a conventional ball mill.

TABLE 2

CHARACTERISTICS OF ELEMENTAL POWDERS

ELEMENT	SOURCE	METHOD OF MANUFACTURE	PURITY	IMPURITIES, W/O	MESH SIZE
ALUMINUM	ALLOY METALS	ATOMIZATION	99.6	Fe-0.19	-140, +325
BISMUTH	——	——	——	——	+80
CHROMIUM	ALLOY METALS	ATOMIZATION	99.7	Fe-0.3	-140, +325
IRON	HOEGANAES CORP	——	98.9	Mn-0.7 Cr-0.26 C-0.15	-100
MANGANESE	ALCAN METALS	——	——	——	-200
MOLYBDENUM	ALLOY METALS	CHEMICAL REDUCTION	99.7	O_2-0.1	-140, +325
NICKEL	ALLOY METALS	ATOMIZATION	99.9	Co-0.05	-140, +325
SILICON	ALCAN METALS	——	——	——	-325
TITANIUM	ALLOY METALS	ATOMIZATION	99.5	Fe-0.23 C-0.12	-140, +325
TITANIUM DIOXIDE	FISHER SCIENTIFIC	——	99.8	WATER SOLUBLE-0.15 SALTS	-325

6-3 DRY POWDER PROCESSING AND SAMPLE PREPARATION

Before inserting the powder charge in the mill, the mill chamber was evacuated and then purged with either argon or nitrogen. The majority of powder systems were processed in a static argon atmosphere at a pressure approximately 10 torr above atmospheric (in order to minimize back diffusion of oxygen into the system during milling), and the powder was then completely discharged from the mill for subsequent analyses. Under certain conditions, however, extremely long discharge times (up to eight hours) were required due to cold welding of the powder to the balls. In such cases, only a representative sample of the powder (minimum 30 percent of the total powder charge) was discharged for analysis. For all powder systems, an argon gas flow rate of 10 cubic ft/hour was maintained during discharge to help prevent oxidation of the milled powder. The unused portion of the powder sample was generally returned to the mill for further processing.

The powders were milled for predetermined time intervals at a given (constant) milling speed and powder-to-ball ratio. The milling parameters chosen for the various alloy systems are listed in Table III. After each selected processing interval, a random sample consisting of approximately 25 grams of the milled powder was withdrawn for analyses. For the X-ray diffractometer scans, a portion of this sample was mounted on a glass slide by means of double-backed Scotch tape.

Another portion was mixed with Lucite powder and heated in a conventional mounting press to obtain a specimen suitable for metallographic examination. The remaining portion of the sample was routinely examined by scanning electron microscopy.

After the final processing interval, randomly chosen samples of the milled powders were sealed off under vacuum in glass ampules and then annealed. The Cr-Mo and oxide free 316 stainless steel powders were annealed for times of the order of 1-3 hours at successively higher temperatures, starting at about 500^{o}C and proceeding on up to a maximum of 750^{o}C. X-ray diffractometer scans were then made on the annealed powders in order to ascertain what structural changes had taken place (due, for example, to the elimination of non-uniform strains) and to determine whether and to what extent homogenization of the samples may have occured as a result of annealing.

6-3a. Slurry Milling

In systems such as the β-Ti alloy and Mn-Bi systems, the tendency toward cold welding (and/or diffusion bonding) is apparently so pronounced that processing under dry conditions at ambient temperatures leads to totally unsatisfactory results. As a possible alternative to dry milling for systems of this kind, attempts were made to mill elemental powder mixtures in the presence of liquid media such as benzene or isoproponal. Type 316 stainless steel powder mixtures were selected for this purpose. After discharge from the mill, the slurry-milled samples were centrifuged at 1500 RPM to promote sedimentation. Most of the liquid was removed by decantation and the remainder was eliminated by evaporation under

TABLE 3

COMPOSITIONS AND MILLING PARAMETERS FOR VARIOUS POWDER SYSTEMS

SYSTEM	WEIGHT %	POWDER CHARGE GRAMS	POWDER/BALL RATIO	MILL SPEED, RPM	MILLING TIME (TOTAL), HRS	MILLING ATMOSPHERE
Cr-Mo	50Cr-50Mo	900	1/17	150	75	argon
	50Cr-50Mo	900	1/17	300	66	argon
316 stainless	65Fe-17Cr-12Ni 3Mo-2Mn-1Si	900	1/17	300	64	argon
		1800	1/8.5	300	103	argon
316 stainless with TiO_2	1 TiO_2	900	1/17	300	96	argon
	2 TiO_2	900	1/17	300	93	argon
	2.5 TiO_2	900	1/17	300	98	argon
	3 TiO_2	900	1/17	300	92	argon
β-Titanium with TiO_2	71Ti-11Cr-8Mn 5Mo-3Al-2TiO_2	900	1/17	300	64	argon
		600	1/25	300	64	argon
Bi-Mn	79Bi-21Mn	560	1/16	150	8	nitrogen
	79Bi-21Mn	560	1/16	300	16	nitrogen

vacuum. Unfortunately, slurry milling also proved unsatisfactory and, in addition, the powders prepared in this fashion were highly pyrophoric.

6-4 CHARACTERIZATION OF THE MECHANICALLY ALLOYED POWDERS

6-4a. X-ray Diffraction Analysis; Structure Determination

Standard X-ray powder diffraction techniques were employed using a General Electric XRD-3 diffractometer equipped with a gas flow counter. Cr K_α radiation was used, a vanadium filter was employed to reduce the intensity of the K_β component to acceptably low levels. The X-ray tube was operated at 35 kV and 15 ma and the diffractometer scans were recorded at a full scale counting rate of 2000 counts/sec.

6-4b. Particle Size and Size Distribution Analysis

Conventional powder screening techniques (i.e., sieving), which rely on the ability of the particles to pass through aperatures of known dimensions, were used to obtain particle size distribution data for the majority of the powder systems investigated here, the one exception being the Cr-Mo powders. These powders were exceptionally fine and were therefore analyzed using a Mine Safety Appliance Particle Size Analyzer. This device relies on the known relationship between the particle settling velocity and particle size (derived from Stoke's law) in order to evaluate the particle size distribution.

6-4c. Particle Morphology or Shape

The shapes or morphologies of the milled powders were evaluated by optical examination of polished cross-sections and by scanning electron microscopy. The SEM (Coates and Welter Field Emission Tip) had a guaranteed resolution of 90 Å and was equipped with a Kevex high-energy dispersive X-ray analyzer.

6-4d. Chemical Homogeneity of the Milled Powder Particles

Several techniques were utilized in an attempt to characterize or evaluate the chemical (as well as structural) homogeneity of the milled powder particles, both before and after annealing. These included analysis of the Bragg profiles (i.e., peak breadths, peak positions and peak or integrated intensities, etc.) on the diffractometer scans, X-ray mapping for specific chemical elements with the EDS unit, metallographic observations on the uniformity of etching of both the milled (cold-worked) and annealed powders, and simple tests to evaluate the magnetic response of the powders (or lack thereof).

Oxide-dispersed (TiO_2) stainless steel and pure iron powders were also prepared by mechanical alloying. To evaluate the uniformity of the oxide distribution, the powders were annealed at high temperatures in order to deliberately coarsen the distribution so that the TiO_2 particles could then be resolved metallographically, This procedure was adopted because it proved to be exceedingly difficult to prepare polished and etched samples of the milled powders in which the oxide particles could clearly be resolved by scanning electron microscopy.

6-5 COLD COMPACTION BEHAVIOR OF MECHANICALLY ALLOYED TYPE 316 STAINLESS STEEL POWDERS

As a side issue to the main investigation, the cold compaction behavior of both oxide-free and TiO_2-dispersed mechanically alloyed Type 316 stainless steel powders was evaluated and compared with prealloyed 316 stainless steel powder. The powders were cold pressed in a floating die and punch arrangement which achieved roughly the same uniformity in pressure distribution as that obtained by doubled ended pressing. The die cavity had the shape of a typical dog-bone tensile specimen and was approximately 1-inch deep. Green compacts weighing approximately 20 grams were prepared under compressive loads of between 70 and 100 ksi (35 to 50 tsi); butyl stearate was used as a die wall lubricant. The green densities of the resulting compacts were calculated from their measured weights in air and from their measured dimensions. The compacts were subsequently impregnated with styrene to which benzoyl peroxide had been added as a polymerization catalyst. After polymerization, the specimens were sectioned and polished for metallographic examination.

7. RESULTS: ANALYSIS AND INTERPRETATION

7-1 Cr-Mo SYSTEM

The primary objective of the experiments which were carried out on this system was to determine if the two elemental components could be interdispersed on something approaching an atomic scale under favorable milling conditions. The only important milling variable investigated was the milling speed. Two separate 900 gram batches of the elemental powders were milled for predetermined times at 150 and 300 RPM respectively. It should be noted that 300 RPM represents the maximum speed and therefore corresponds to the maximum energy input rate obtainable with the particular attritor mill used in this work. Aside from the milling speed, all other processing parameters such as the powder-to-ball ratio and the milling atmosphere were held constant (see Table 3).

Beginning with the original mixture of the elemental powders, the changes in the X-ray diffraction spectra which take place when the powders are milled for successively longer times at 150 RPM are shown in Figure 13. The two most prominent or most intense Bragg peaks in the original powder mixture are those corresponding to diffraction from (110) planes in bcc Mo and Cr; these peaks occur at $2\theta=61.9^{\circ}$ for pure Mo and at $2\theta=68.3^{\circ}$ for pure Cr. Although the entire diffraction spectrum was recorded in each case, only the portions of the diffractometer scans between about 55° and 75° 2θ are reproduced in Figure 13. As it turns out, this is the only part of the diffraction spectrum from which much information can be extracted because all of the other elemental peaks, such as the (200) and (211) reflections, which occur at higher Bragg angles, are almost completely obliterated by cold work as milling proceeds.

It is immediately apparent from Figure 13 that the two elemental (110) Bragg peaks are progressively broadened and reduced in intensity as time proceeds. Closer inspection reveals, that within the uncertainty to which the positions of the Bragg peaks can be measured from the diffractometer charts which is conservatively estimated to be within $\pm$ 0.05° 2θ, the elemental Cr (110) peak at 68.3° and the elemental Mo (110) peak at 61.9° 2θ both remain completely unshifted. Since the integrated intensity between 55° and 75° 2θ is mainly due to these two Bragg peaks, it can be concluded with reasonable assurance that, even after milling for times as long as 75 hours at 150 RPM, the powders still consist largely (but, as will be seen, perhaps not entirely) of mechanical mixtures of the two pure components. This has been confirmed to some extent by microscopic examination of polished cross-sections of the powder samples. Thus, after 75 hours of processing, relatively large angular Cr fragments could still be detected in the powder mixture (see Figure 20b); however, because the Mo fragments were considerably smaller, they were much more difficult to identify with certainty.

The peak intensities (measured relative to the original powder mixture) and peak breadths (full width at half-maximum intensity) were determined after each processing interval. The values obtained are listed in Table 4 . It may be observed that the reduction in peak intensity and the amount of broadening are both substantially

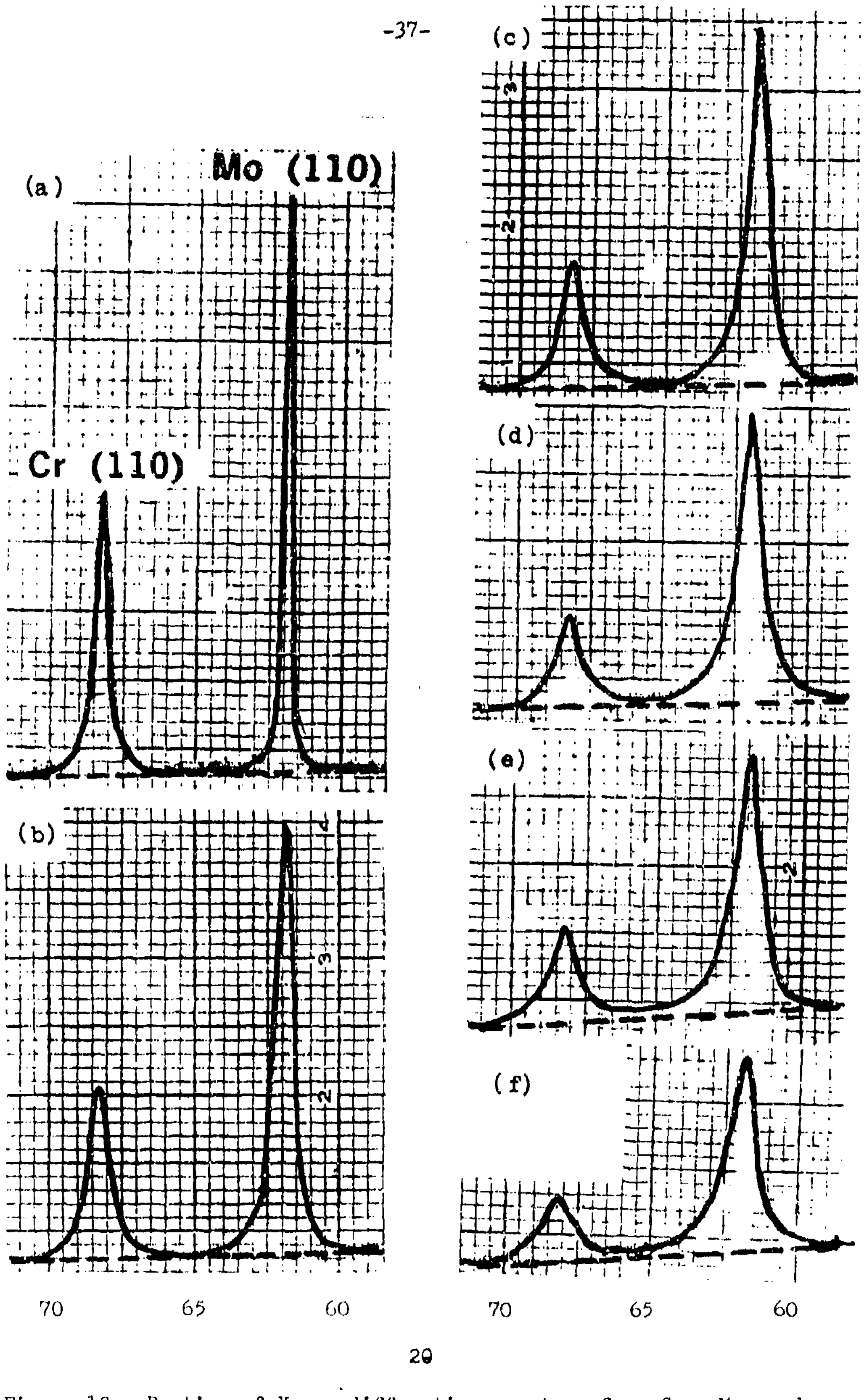

Figure 13 - Portion of X-ray diffraction spectrum from Cr - Mo powders milled at 150 RPM: a) unmilled mechanical mixture, b) milled for 7 hours, c) milled for 19 hours, d) milled 38 hours, e) milled 52 hours, and f) milled for 75 hours.

TABLE 4

PEAK INTENSITY AND PEAK BREADTH MEASUREMENTS
CHROMIUM - MOLYBDENUM SYSTEM

MILLING TIME AT 150 RPM, HRS	Mo (110) RELATIVE INTENSITY, I/I_o	Mo (110) FWHM*, 2θ DEGREES	Cr (110) RELATIVE INTENSITY, I/I_o	Cr (110) FWHM*, 2θ DEGREES
0	1.0	0.5	1.0	0.6
2	0.98	0.5	0.65	0.9
7	0.78	0.8	0.62	0.9
13	0.74	0.8	0.59	1.0
19	0.64	0.8	0.40	1.2
27	0.62	0.9	0.38	1.2
32	0.52	1.0	0.35	1.3
38	0.48	1.1	0.30	1.5
45	0.45	1.1	0.25	1.5
52	0.42	1.1	0.23	1.5
75	0.31	1.1	0.20	1.6

MILLING TIME AT 300 RPM, HRS	Mo (110) RELATIVE INTENSITY, I/I_o	Mo (110) FWHM*, 2θ DEGREES	Cr (110) RELATIVE INTENSITY, I/I_o	Cr (110) FWHM*, 2θ DEGREES
0	1.0	0.5	1.0	0.6
2	0.69	0.7	0.45	1.1
7	0.62	0.9	0.38	1.2
13	0.36	1.1	0.25	1.3
19	0.28	1.2	0.20	1.3
27	0.26	1.2	0.15	1.5
34	0.17	1.4	0.15	1.6
50	0.12	1.5	0.13	1.9
65	0.09	1.7	0.09	2.0

*Full width at half-maximum intensity

greater for the elemental Cr (110) Bragg peak than for the Mo (110) peak. This holds throughout the milling cycle, but is especially noticeable during the early stages of processing. The clear implication is the elemental Cr particles (or processed Cr fragments within composite particles) are being deformed and work-hardened to a greater extent by impact collision with the balls than are the Mo particles. This may be related as much to differences in the physical nature of the original metal powders as to differences in the inherent work hardening characteristics of the two metals. The Cr powder was prepared by atomization and the individual Cr particles are relatively dense; the Mo powder, on the other hand, was prepared by chemical reduction and is very spongy, which, no doubt, makes it much more friable (see Figure 20a).

When the diffractometer scans in Figure 13 are examined in greater detail, some rather subtle but perhaps meaningful changes of a different nature can be observed as the powders are processed for longer and longer periods of time. For example, after only about 19 hours of milling it is apparent that the diffraction intensity in the region between the two elemental peaks no longer falls to background level but becomes finite. This is even more evident after 38 hours of milling, by which time the two elemental peaks have also become noticeably asymmetrical. Continued processing does not substantially raise the intensity level between the two elemental peaks beyond that produced by milling for 38 hours. The simplest or most obvious explanation for why the intensity does not fall to background level between the two peaks is the elemental Bragg peaks eventually become broadened to such an extent, due to non-uniform strains introduced by cold work or particle size broadening, that the tails of the two peaks begin to overlap. However, another explanation is also possible. It is precisely in the intermediate region between the two elemental Bragg peaks where we would expect the diffraction intensity to be high if solid solutions near 50 w/o Cr - 50 w/o Mo were being formed.

Although a clear distinction between these two interpretations cannot be made for the powders milled at 150 RPM, an unambiguous interpretation is possible in the case of the Cr-Mo powders milled at 300 RPM, as will shortly be demonstrated. There is little doubt that solid solutions are formed on milling at 300 RPM. The possibility that some interdispersion of the two elemental components on a scale approaching atomic dimensions may also have taken place on milling for long times at 150 RPM cannot, therefore, be entirely dismissed. Indications that this may actually be so have been derived from the results of annealing studies on these powders.

The changes in the X-ray diffraction spectra which occur when Cr-Mo powders that have been milled for 75 hours at 150 RPM are annealed for short times (1.5 hr) at temperatures between 500° and $750^{\circ}C$ are shown in Figure 14. Not only do the elemental Bragg peaks sharpen up, as expected, due to the relief of non-uniform internal strains, but a surprising amount of "fine structure" eventually develops in the region between these two peaks (i.e., between about 63° and 67° 2θ) even though the elemental peaks remain unshifted. The sharply-defined peak at $2\theta=65.8^{\circ}$ (corresponding to ≈ 44 w/o Mo) which emerges after annealing at $750^{\circ}C$ is particularly noteworthy. The integrated intensity in the region between about 63° and 67° 2θ constitutes a sizeable fraction of the total integrated intensity in the powder sample annealed at $750^{\circ}C$. Bragg angles between 63° and 67° 2θ encompass the composition range between about 20 w/o Cr - 80 w/o Mo and 75 w/o Cr - 25 w/o Mo (or 30 a/o Cr to 85 a/o Cr) according to published lattice-parameter vs. composition data (see Table I and Figure 12).

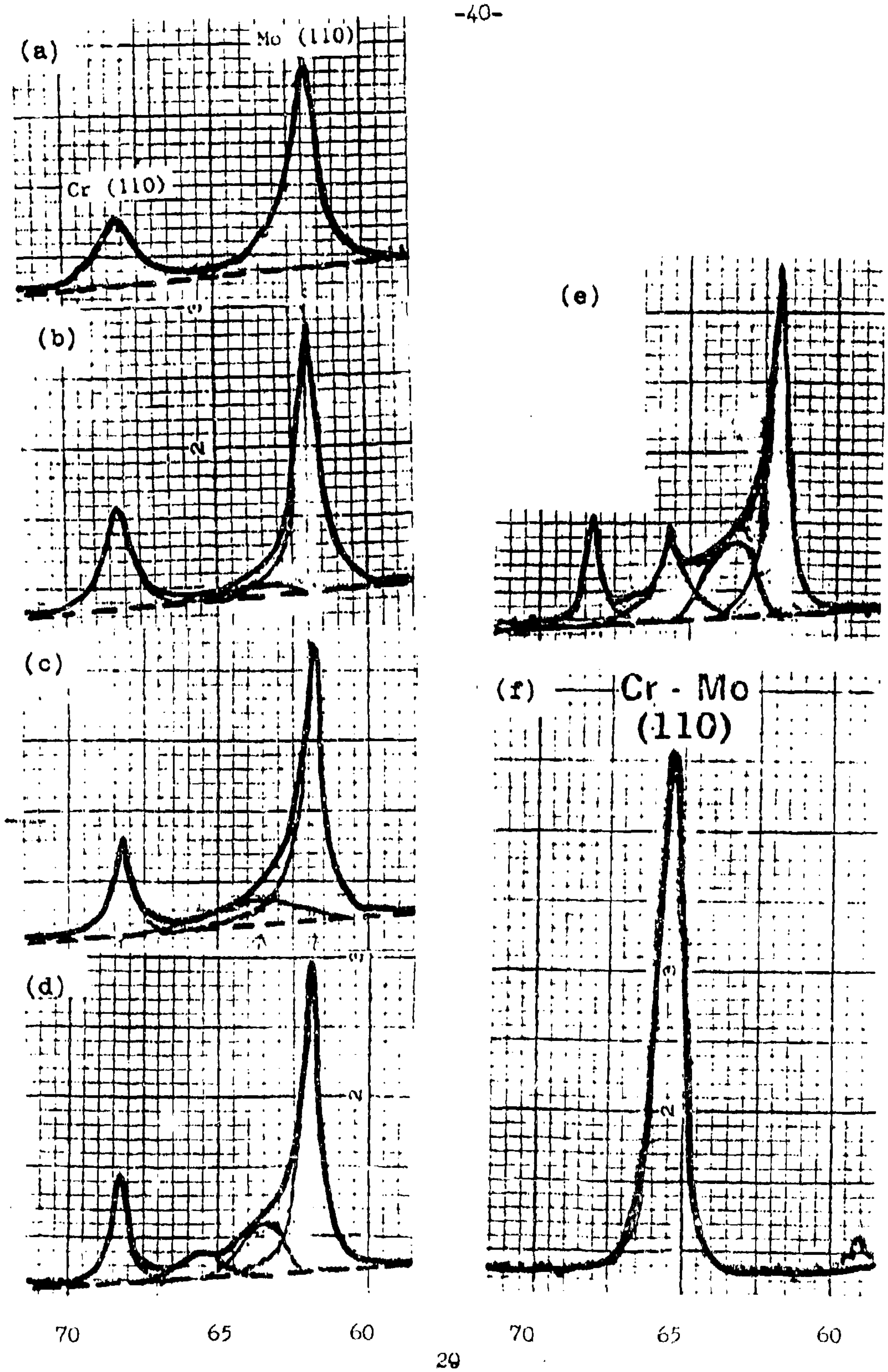

Figure 14 - Portion of X-ray diffraction spectrum from Cr - Mo powders milled at 150 RPM for 75 hours and then annealed: a) unannealed b) 1.5 hr at 500°C, c) 1.5 hr at 575°C, d) 1.5 hr at 650°C, and e) 1.5 hr at 750°C. The diffraction spectrum from the homogenized Cr - Mo casting is shown in f).

It is clear that substantial changes in chemical composition (as well as structual changes) have occurred as a result of annealing, although it is difficult to define these precisely. The maximum annealing temperature of 750°C or 1023°K corresponds to only 0.35 T_m for Mo and 0.48 T_m for Cr (or approximately 0.44 T_m for the 50/50 w/o alloy). Since the annealing temperature is quite low, compared to the respective melting temperatures, only short-range diffusion could have taken place during the anneal. Solute diffusion data are not available for the Cr-Mo system, but the tracer or self-diffusion coefficient for both polycrystalline Cr and Mo have been measured at high temperatures[25,26]. These data, when extrapolated to 1023°K, give $D \approx 10^{-21}$ cm²/sec for Mo and $D \approx 4 \times 10^{-17}$ cm²/sec for Cr. Taking the higher of these two values, so as to be more conservative, and using the random-walk relationship, $\bar{x}^2 = 2Dt$, the average diffusion distance (or rms displacement) during a 1.5 hour anneal at 1023°K is estimated to be less than 100Å. This indicates that some powder particles may be present after milling at 150 RPM in which the two elemental components are dispersed on a dimensional scale of this same order or smaller.

The results obtained on milling at 150 RPM may be summarized by referring to Figure 15, in which the diffractometer scan for the Cr - Mo powder milled for 75 hours is compared with that for unmilled mechanical mixture and that for the chemically homogeneous arc-cast reference standard. The diffractometer scan for the annealed powder (1.5 hour at 750°C) is also included in Figure 15 for completeness. It may be seen that the diffraction pattern for the milled powder bears a much closer resemblance to that for the original elemental mixture than that for the homogenous solid solution alloy. This establishes that the milled powders consist largely of mechanical mixtures of the two elemental components. However, the compositional changes which occur on annealing are interpreted as evidence that interdispersion of the ingredients on a scale of less than 100Å has taken place in an appreciable fraction of the powder particles.

The changes in the X-ray diffraction spectra which occur when the elemental Cr-Mo powder mixture is milled for successively longer times at 300 RPM are illustrated in Figure 16. Compared to the behavior at 150 RPM, much more rapid and more pronounced changes are observed in peak intensity, peak breadth and peak shape as the processing time increases. This is consistent, of course, with the higher energy input rate associated with the higher milling speed. The relative intensities and breadths of the elemental Cr (110) and Mo (110) Bragg peaks after various processing times at 300 RPM are listed in Table 4 . When compared with corresponding data listed in the same table for powders milled at 150 RPM, the more rapid processing rate at 300 RPM becomes obvious. As before, it appears that the elemental Cr particles are being processed somewhat more rapidly or extensively than the Mo particles, especially during the early stages. It also appears, although this is difficult to establish with complete certainty, that the positions of the elemental Bragg peaks do not shift significantly as time proceeds. This indicates that even after milling for periods as long as 65 hours, individual particles (or relatively large fragments within composite particles) consisting essentially of pure Mo and pure Cr are still present. However, the proportion of these particles is much smaller than at 150 RPM.

The most significant feature of the diffraction spectra in Figure 16, and what distinguishes them from the corresponding diffractometer scans on powders milled

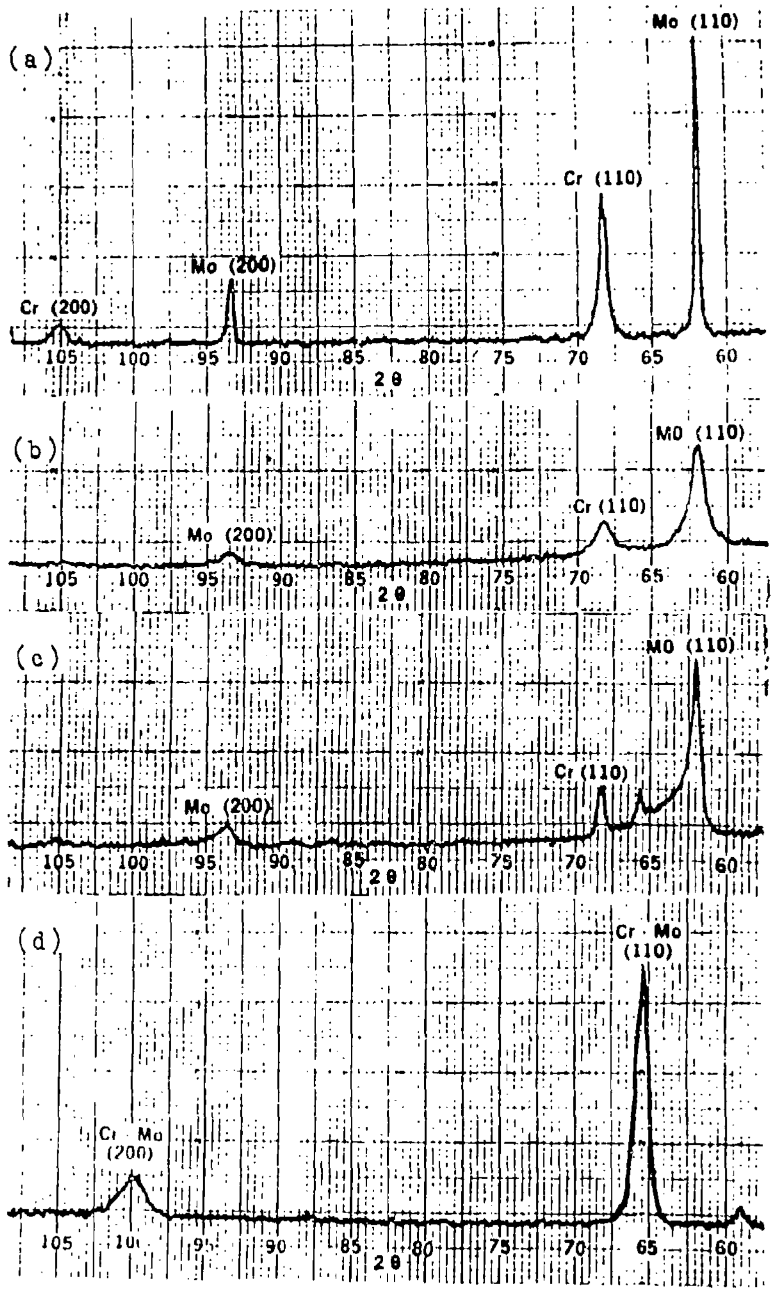

Figure 15 - X-ray diffraction spectra from Cr - Mo powders: a) unmilled mechanical mixture, b) milled for 75 hours at 150 RPM, c) same as (b), but annealed for 1.5 hours at 750°C, d) arc-cast and homogenized Cr - Mo alloy.

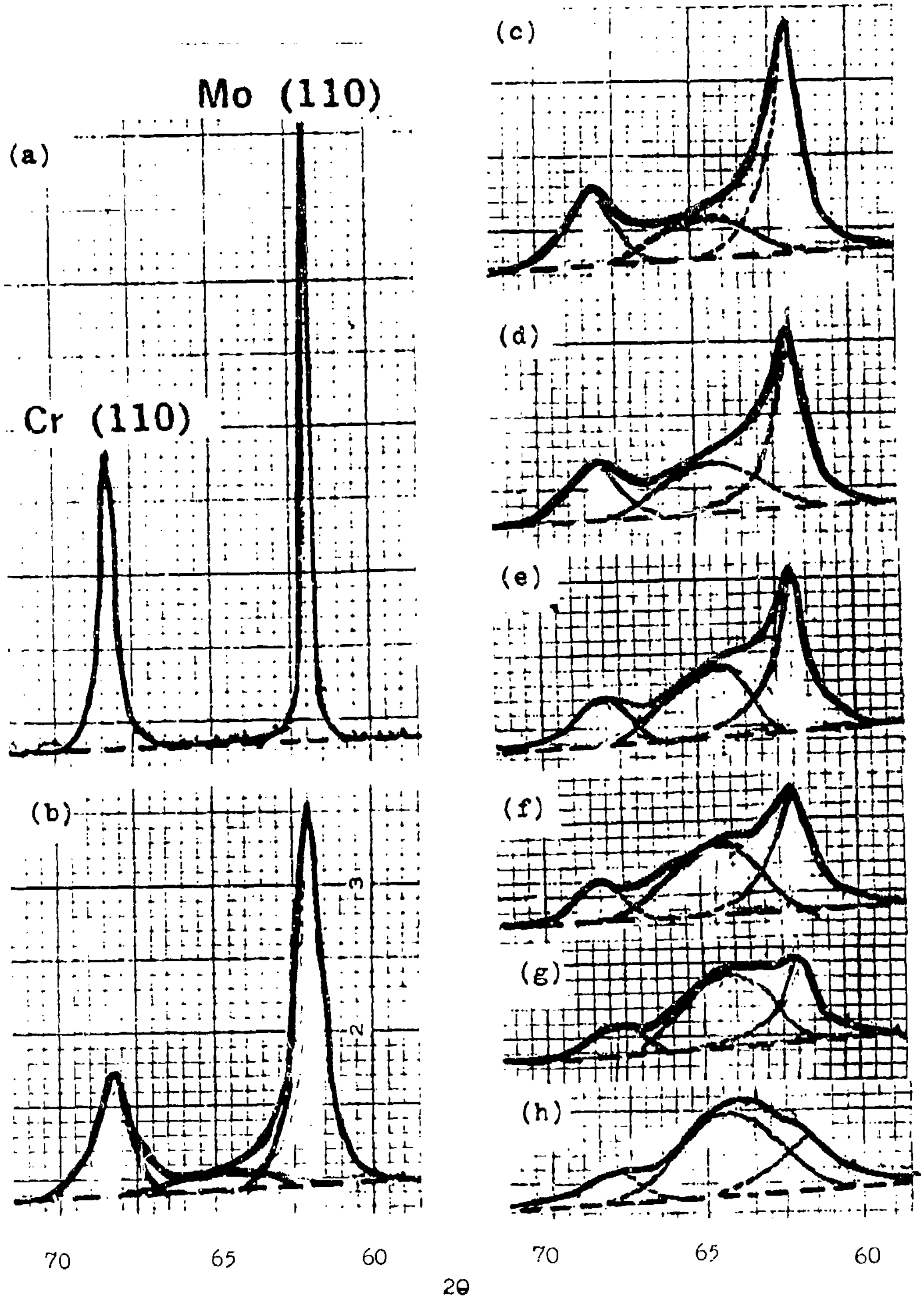

Figure 16 - Portion of X-ray diffraction spectrum from Cr - Mo powders milled at 300 RPM: a) unmilled mechanical mixture, b) milled 7 hours, c) milled 13 hours, d) milled 19 hours, e) milled 27 hours, f) milled 34 hours, g) milled 50 hours, and h) milled milled 65 hours.

at 150 RPM (Figure 13), is that the diffraction intensity in the region between the two elemental peaks is much greater and also increases dramatically as processing continues (with a corresponding reduction of the elemental peak intensities). After 65 hours of milling, for example, a broad but clearly defined peak is present at about 64.5° 2θ. Analysis of the shape of the diffraction profile between the two elemental (110) Bragg reflections indicates that this broad peak, centered at about 64.5° 2θ, developed gradually with time. It was definitely present after milling for 27 hours and most probably well before, as subsequent discussion will show. It is not possible to account for the presence of this peak simply by overlapping the tails of the strain-broadened elemental peaks. The only logical interpretation is that this peak arises from powder particles in which the two components are intimately mixed on an atomic scale, and can therefore be regarded as being in true solid solution.

Assuming this interpretation is correct and the strain-broadened elemental Bragg peaks remain symmetrical, it is possible to decompose the observed spectra in the region between about 55° and 75° 2θ into three separate components, or three groups of particles as shown in Figure 16. When this is done it is found that a broad "solid-solution" peak centered at about 64.5° 2θ can already be identified after as little as 7 hours of processing. This peak grows in intensity but does not become significantly broader as time increases. Furthermore, the center of this peak stays very close to 64.5° 2θ throughout the entire milling cycle. This peak apparently corresponds to the (110) reflection from bcc Cr-Mo solid solutions. The fact that the peak is so broad, compared to the two elemental peaks, indicates that the solid solutions are chemically very inhomogeneous (or that chemically homogeneous particles having a broad range of compositions are present, which is far less likely). If the solid solution were homogeneous, a Bragg angle of 64.5 2θ for the (110) reflection would correspond to a composition very close to 60 w/o Mo - 40 w/o Cr (or 45 a/o Mo - 55 a/o Cr).

The integrated intensities under the three component (110) peaks (corresponding to Mo, Cr and inhomogeneous solid solution alloy powder particles) were determined graphically from Figure 16. The fraction of the total integrated intensity contained under each of these three peaks is plotted as a function of processing time in Figure 17. It is noteworthy that, after milling for 65 hours, roughly 70% of the total integrated intensity is due to the solid solution peak, indicating that the largest proporation of the particles now consist of alloy particles rather than elemental fragments. It also appears that the rate of processing may slow down slightly as time proceeds but this can by no means be regarded as well established. A rough comparison can also be made between the powders milled at 150 RPM and 300 RPM, insofar as processing rate is concerned. The diffractometer scan for powders milled for 75 hours at 150 RPM is basically similar to that for powders milled for 7 hours or less at 300 RPM. Thus, increasing the milling speed from 150 to 300 RPM has increased the processing rate by at least an order of magnitude.

The evidence that true solid solutions, although admitedly very inhomogeneous chemically, are formed by milling elemental Cr and Mo powders at 300 RPM appears to be fairly convincing. Since the phase diagram for this system (see Figure 11) indicates the presence of a miscibility gap at low temperatures, the solid solutions formed by mechanical alloying must be metastable. Phase separation might

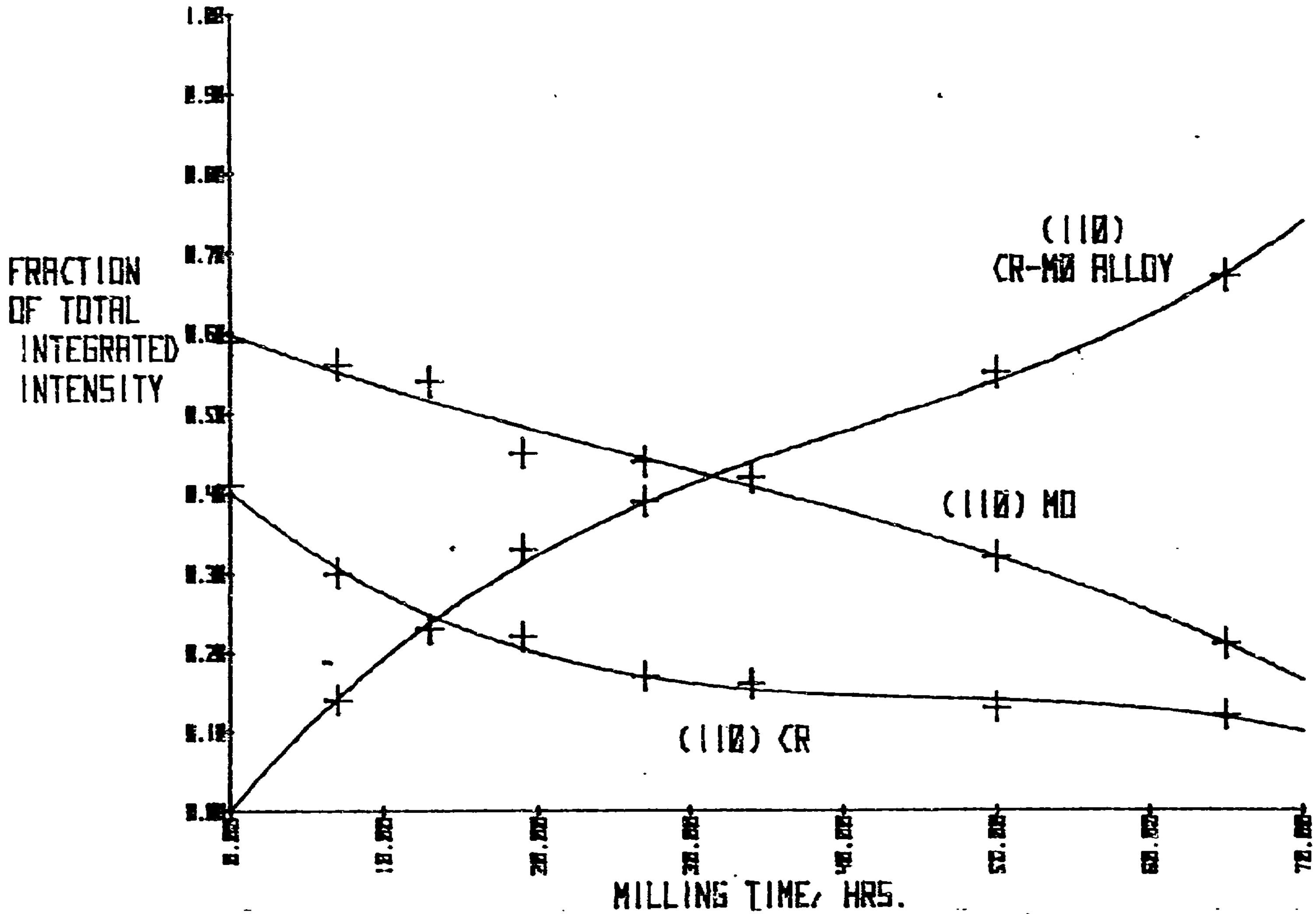

Figure 17 - Fraction of total integrated intensity under the three Cr - Mo component peaks as a function of processing time (mill speed - 300 RPM).

therefore be expected to occur when the milled powders are annealed at temperatures which place the overall composition, i.e., 50 w/o Cr - 50 w/o Mo, within the miscibility gap. This does not seem to be borne out in practice. The diffractometer scans obtained on powders milled for 65 hours at 300 RPM and then annealed for 1.5 hours at temperatures between 500° and 750°C are shown in Figure 18. The solid solution or alloy peak at about 64.5° 2θ narrows considerably and increases in intensity on annealing at higher and higher temperatures (refer also to Table 5), presumably due to a combination of strain-relief and homogenization. After annealing at 750°C, a subsidiary peak seems to have developed on the high-angle side of the alloy peak at about 2θ=65.8°. It may be recalled that a sharply-defined peak was observed at this same angle in the powder sample milled at 150 RPM after annealing at 750°C. Unfortunately, these annealing experiments were not carried far enough to determine whether or not a completely homogeneous solid solution alloy powder could eventually be produced by annealing for long times at 750°C.

The results obtained on milling at 300 RPM may be summarized by referring to Figure 19, in which the diffractometer scan for the Cr-Mo powder milled for 65 hours is compared with that for the unmilled mechanical mixture and that for the chemically homogeneous arc-cast reference standard. Also included in this figure is the diffractometer scan for the milled powder after annealing at 750°C. It may be seen that in contrast to the powder milled at 150 RPM, the diffraction pattern for the powder processed at 300 RPM bears a much closer resemblance to that for the homogeneous solid solution alloy than that for the original elemental powder mixture. This establishes that the two elemental components have indeed become interdispersed on an atomic scale as a result of high-energy milling. However, the breadth of the solid solution or alloy peaks as well as the compositional changes which occur on annealing both provide strong indication that the solid solutions formed by high-energy milling are very inhomogeneous from a chemical and structual point of view.

We may conclude this section with some brief observations concerning particle shape, particle size and particle size distribution. Photomicrographs of polished cross-sections of the unmilled mechanical mixture are shown in Figure 20a. The spongy or porous nature of the original Mo particles, mentioned previously, is clearly apparent. Corresponding photomicrographs for powders milled at 150 RPM and at 300 RPM are presented in Figure 20b and Figure 20c respectively. These photographs illustrate the magnitude of the particle size reduction obtained by high-energy milling in this system. The particles in both batches of powder were found to have nearly equiaxed shapes, (except for the angular chromium fragments in the powder milled at 150 RPM), as may be seen from Figure 21. The particle morphology in this system is basically similar to that obtained by Benjamin in the Fe-Cr system[18].

Particle size analyses for the two powder batches are given in Table 6. The majority of the powder particles in both batches were less than 40μm in diameter. Only 5% by weight of the particles in the powder milled for 65 hours at 300 RPM were larger than 40μm, in fact. In comparison, 27% by weight of the particles were larger than 40μm in the powder batch milled for 75 hours at 150 RPM. Milling at 300 RPM also led to a somewhat narrower size distribution, as might be expected.

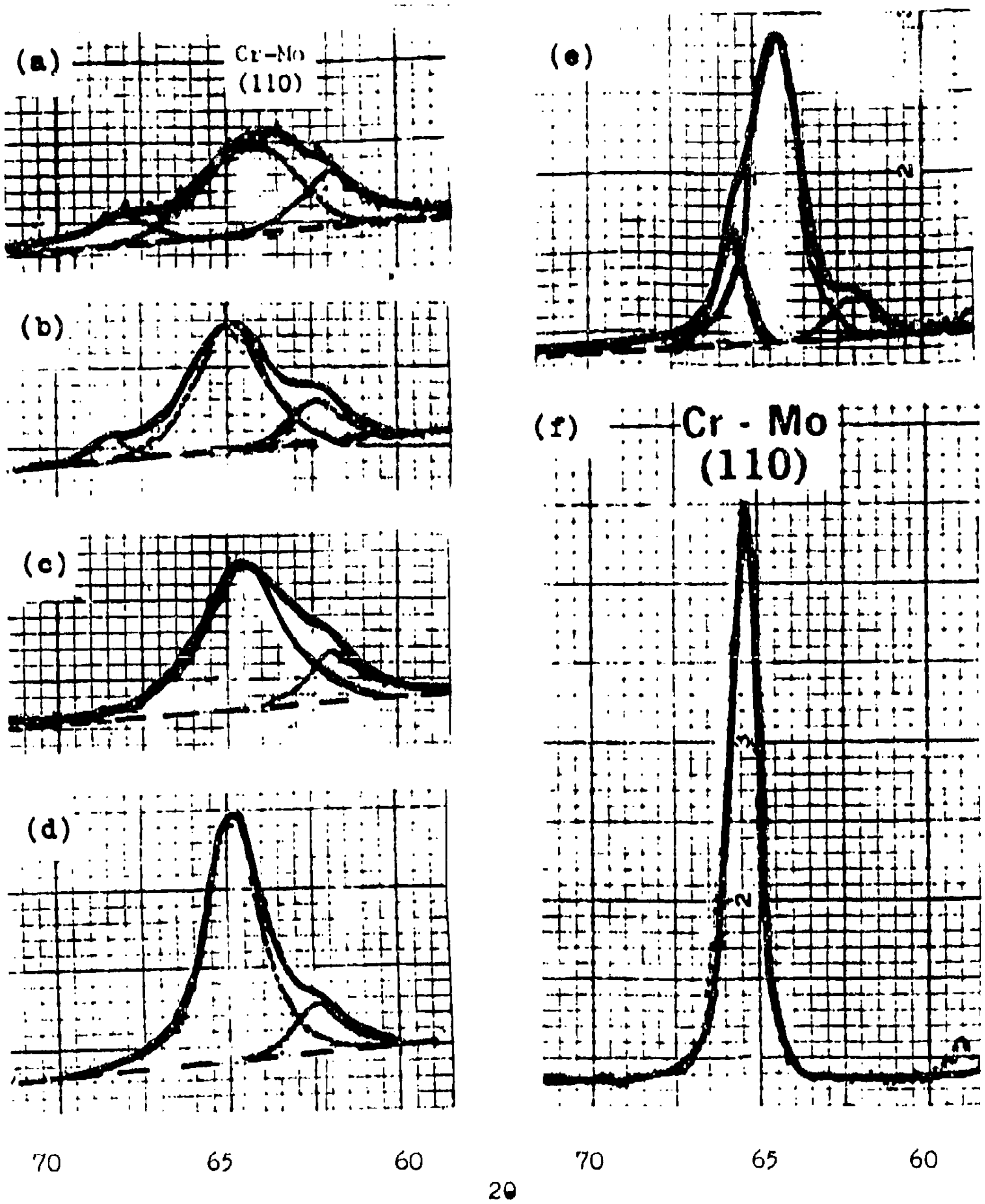

Figure 18 - Portion of X-ray diffraction spectrum from Cr - Mo powders milled at 300 RPM for 65 hours and then annealed: a) unannealed, b) 1.5 hr at 500°C, c) 1.5 hr at 575°C, d) 1.5 hr at 650°C, and e) 1.5 hr at 750°C. The diffraction spectrum from the homogenized Cr - Mo casting is shown in f).

TABLE 5

THE EFFECT OF ANNEALING TEMPERATURE ON THE PEAK INTENSITY AND WIDTH OF THE (110) BRAGG REFLECTION IN MECHANICALLY ALLOYED Cr-Mo POWDERS

ANNEALING TEMPERATURE, °C*	RELATIVE INTENSITY, I/I_o	FWHM 2Θ, DEGREES
As-milled (65 hours at 300 RPM)	0.20	4.2
500°C	0.25	4.0
575°C	0.27	3.8
650°C	0.45	2.3
750°C	0.57	1.6
Homogenized Arc-Cast Alloy	1.0	0.9

*Annealing time = 1.5 hours at all temperatures.

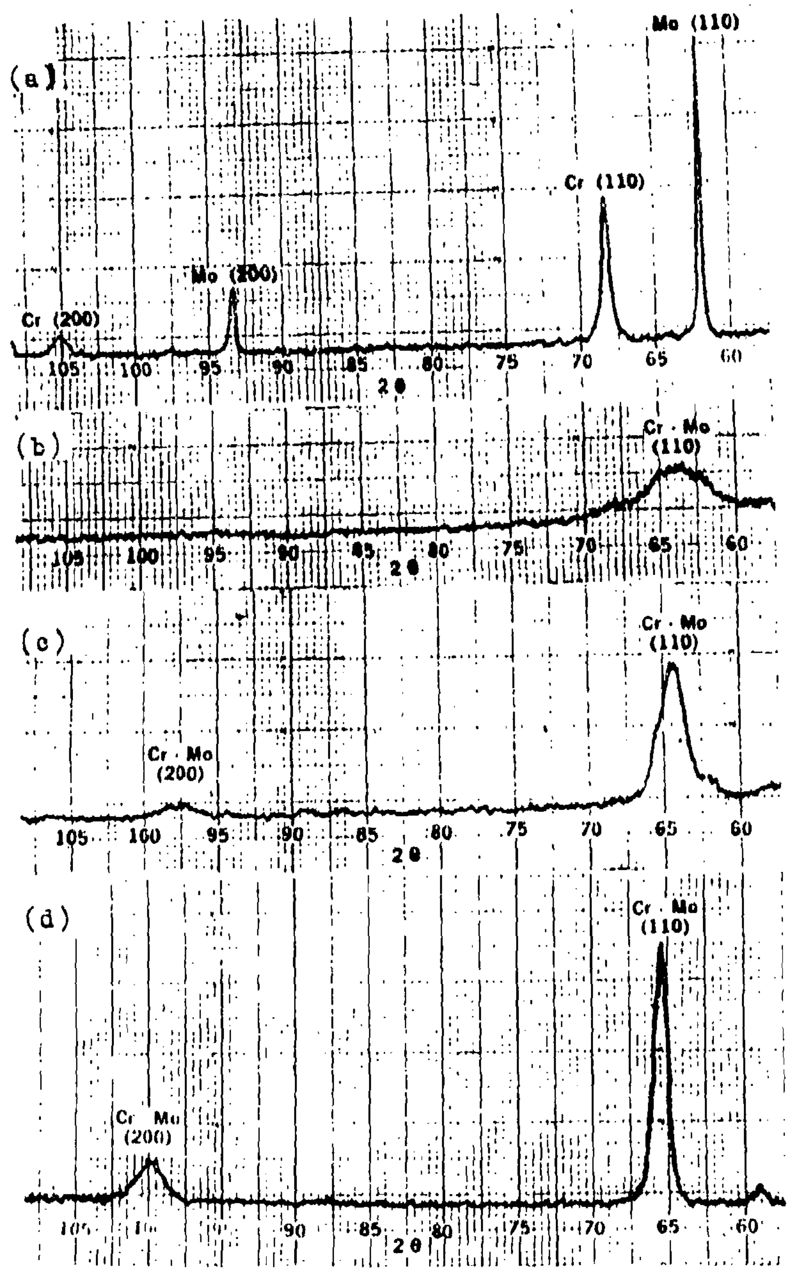

Figure 19 - X-ray diffraction spectra from Cr - Mo powders: a) unmilled mechanical mixture, b) milled for 66 hours at 300 RPM, c) same as (b), but annealed 1.5 hours at 750°C, d) arc-cast and homogenized Cr - Mo alloy.

(a)

(b)

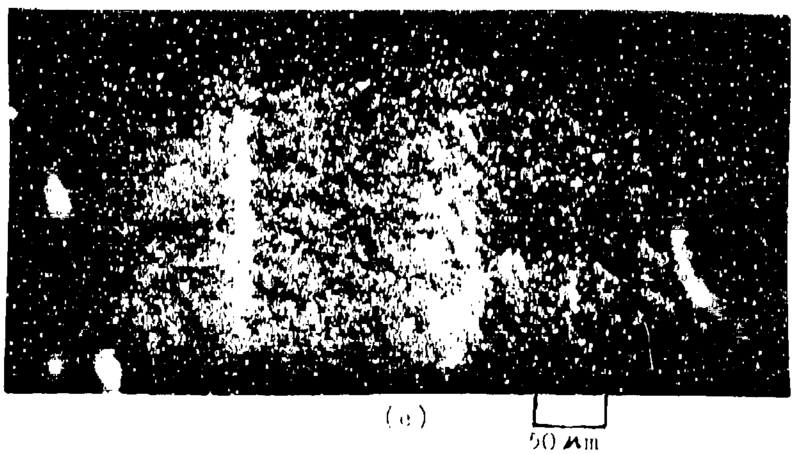

(c)

Figure 20 - Polished and unetched cross sections of Cr - Mo powders: a) unmilled powder mixture, Cr (white), Mo (speckled due to porosity), b) milled 75 hours at 150 RPM, c) milled 65 hours at 300 RPM, unetched. (X 200)

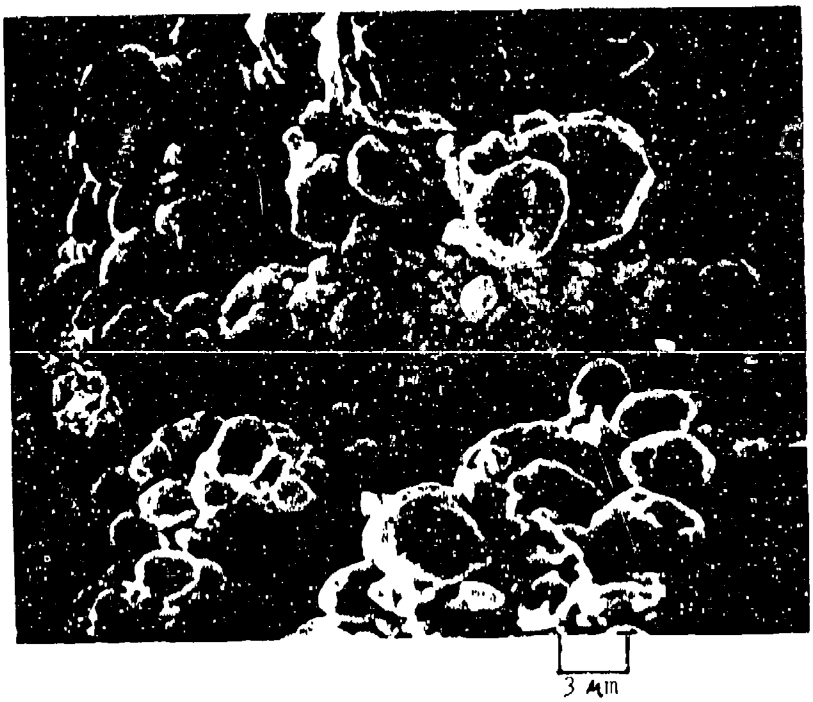

Figure 21 - SEM micrograph of the Cr - Mo powder milled for 65 hours at 300 RPM (X3000).

TABLE 6

PARTICLE SIZE ANALYSES* OF MECHANICALLY ALLOYED
CHROMIUM-MOLYBDENUM POWDERS

PARTICLE SIZE RANGE, μm	PERCENTAGE BY WEIGHT 75 HRS @ 150 RPM	65 HRS @ 300 RPM
+80	1	0
-80, +60	7	1
-60, +40	19	4
-40, +20	39	39
-20, +10	15	35
-10, +5	13	17
-5	6	4

*As determined using a Mine Safety Appliance Particle Size Analyzer

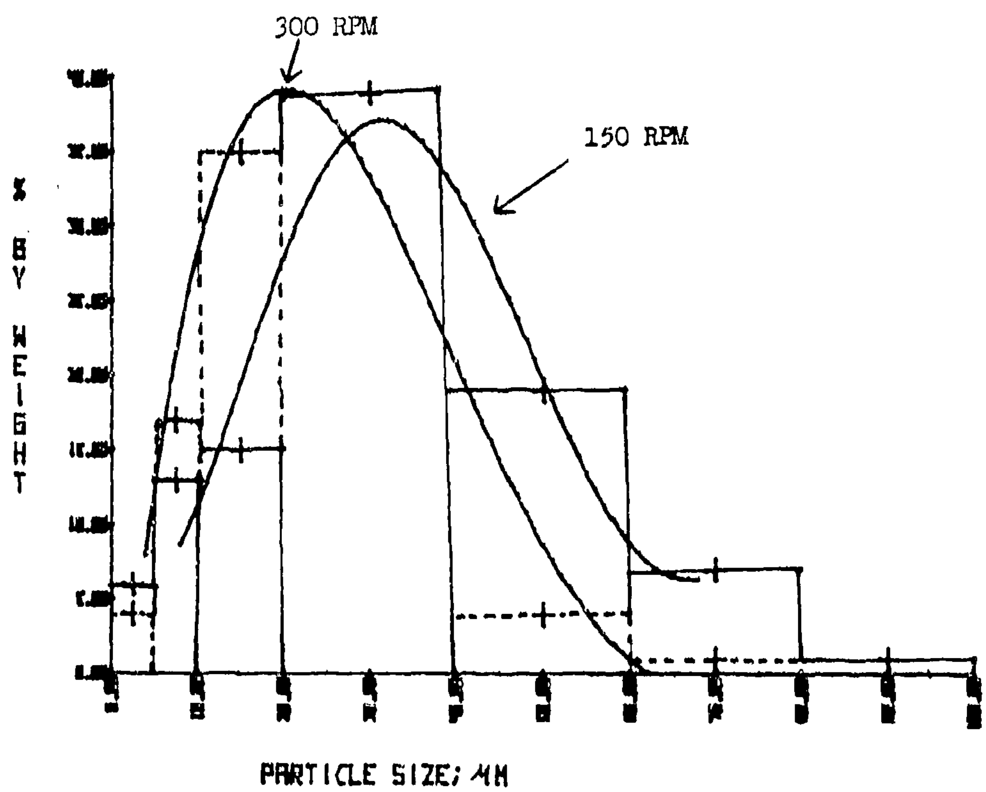

In this series of experiments, the primary interest again was in establishing whether or not high-energy milling of a mechanical mixture of the elemental powders (in this case six different elemental powders with four different crystal structures) could result in the formation of a single, structurally homogeneous alloy solid solution powder (fcc) under favorable conditions. The only milling variable investigated was the powder-to-ball ratio; the milling speed was held constant at 300 RPM (see Table III). Experiments were also carried out to determine the effects that additions of TiO_2 in amounts of between 1-3 w/o have on the rate of powder processing, i.e., on the extent of alloy formation. The cold compaction behavior of both oxide-free and oxide-dispersed mechanically alloyed 316 stainless steel powders was also investigated and compared with that of a prealloyed 316 stainless steel powder.

7-2a. Oxide-Free Powders

A 900 gram batch of the elemental powder mixture (17Cr-12Ni-3Mo-2Mn-1Si-balance Fe) was milled at a powder-to-ball ratio of 1:17 for times of 16, 32, 48 and 64 hours under argon. A portion of the diffractometer scan obtained on the powder milled for 16 hours is shown in Figure 22 along with that for the original powder mixture and that for prealloyed 316 stainless steel powder. After only 16 hours of milling, all of the elemental Bragg peaks appear to have been obliterated (or so severely broadened as to escape detection) except for the (110)*, (200) and (211) α-Fe reflections at $2\theta=68.7^{\circ}$, 106.1° and 156.3°, respectively. All of the remaining elemental peaks were significantly broadened, however. Three additional peaks, which do not correspond to any of the elemental components, were also present, viz., a relatively intense peak at $2\theta \cong 67^{\circ}$ and two peaks of lower intensity at $2\theta \cong 79^{\circ}$ and $2\theta \cong 128^{\circ}$.

Comparison of the diffraction spectrum with that for the prealloyed 316 stainless steel powder (Figure 22d) indicates that these new peaks correspond, respectively, to the (111), (200), and (220) reflections from a fcc solid solution having approximately the same lattice constant, and hence approximately the same composition, as Type 316 stainless steel. The relative intensities of these three peaks are also consistent with this interpretation. Thus, it appears that after only 16 hours of processing, the elemental components have become interdispersed on an atomic scale and that extensive alloy formation has occurred. It is also evident, compared to Cr-Mo powders, the stainless steel powder mixture is being processed at a much faster rate under basically equivalent conditions.

---

*In the diffraction spectrum of the unmilled mechanical mixture of elemental powders, the (110) α-Fe, (110) Cr, and (111) Ni reflections, at $2\theta = 68.7^{\circ}$, 68.3°, and 68.4° respectively, are superimposed. That is, they are not resolved and therefore give rise to a single (relatively sharp) peak at $2\theta = 68.7^{\circ}$. Since α-iron is the major component, this combined peak at $2\theta = 68.7^{\circ}$ will hence forth be referred to as the (110) α-Fe peak.

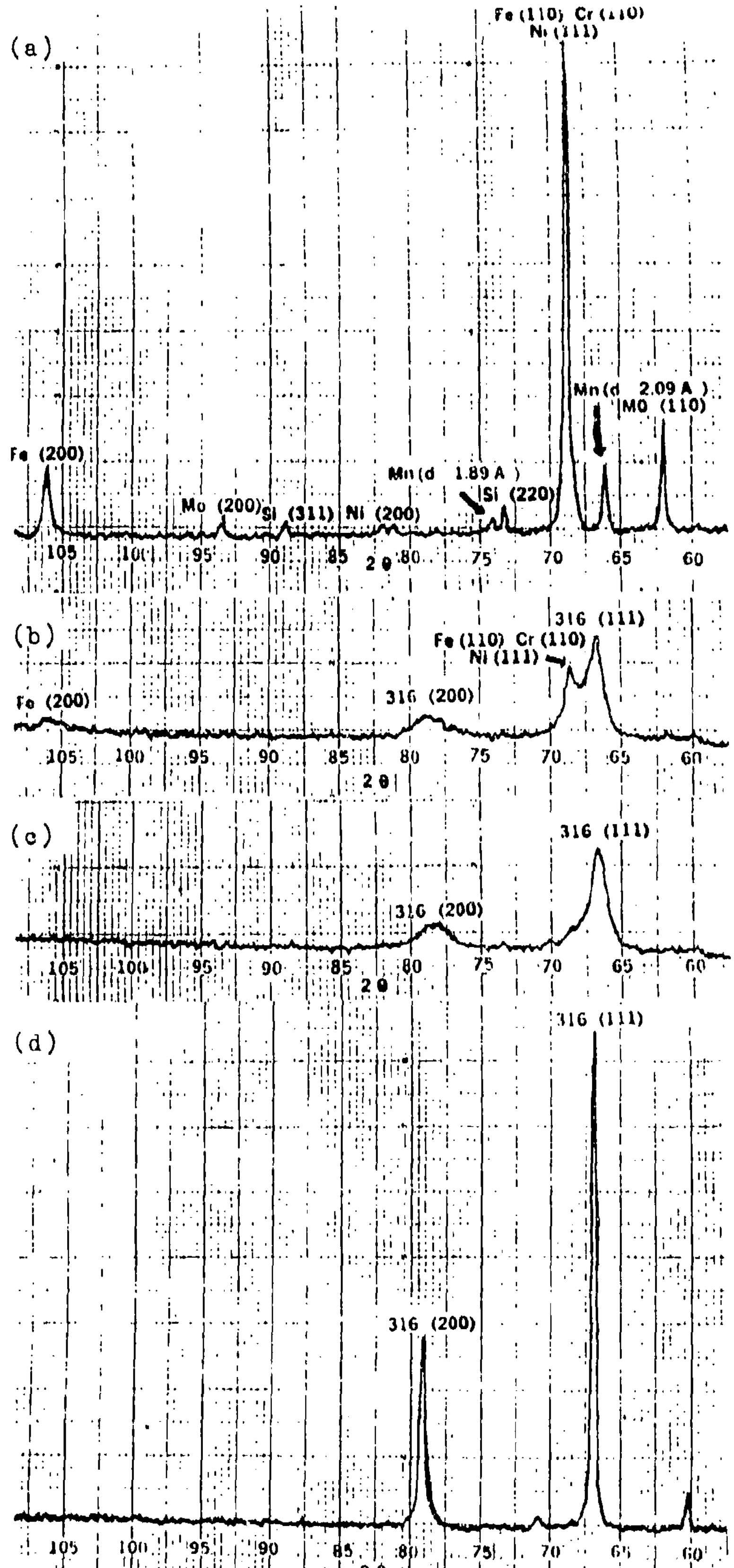

Figure 22 - X-ray diffraction spectra from Type 316 stainless steel powder mixtures (1:17 powder-to-ball ratio): a) unmilled mechanical mixture, b) milled for 16 hours at 300 RPM, c) milled for 32 hours at 300 RPM, d) prealloyed 316 stainless steel powder.

After 32 hours of milling, the (200) and (211) reflections from α-Fe were also eliminated; only the three broadened peaks characteristic of the fcc solid solution alloy plus the α-Fe (110) peak, though now of substantially reduced intensity, were present (see Figure 22c). The (110) α-Fe reflection completely disappeared after an additional 32 hours of milling (64 hours total) so only the three broadened solid solution alloy peaks remained (Figure 23a). Almost complete interdispersion of the ingredients has therefore been obtained after 64 hours of processing.

The relative peak intensities of two of the most prominent peaks in the diffraction spectrum after various milling times are listed in Table 7. These two peaks correspond to the α-Fe (110) reflection from the elemental powders and to the (111) reflection from the fcc solid solution alloy powder; the corresponding peak widths are also listed in this table. The intensity and sharpness of the fcc alloy diffraction peaks increased when the milled powders were annealed for 1 hour at temperatures between 500°C and 650°C (Table 7). Of greater significance, however, is the observation that distinct peak shifts also occurred for all three fcc reflections, clearly indicating that the milled powders were not chemically homogeneous. The magnitudes of these peak shifts ($\Delta 2\theta$), are given in Table VIII. The diffractometer scan obtained on the powder milled for 64 hours after annealing for 1 hour at 650°C is shown in Figure 23b. The close similarity between this pattern and that for the prealloyed stainless steel powder is evident.

Increasing the powder-to-ball ratio from 1:17 to 1:8.5 substantially increased the time necessary for the formation of an alloy powder. Thus, even after 64 hours of milling at 300 RPM, the elemental α-Fe peak at $2\theta = 68.7°$ was still present, although all other elemental peaks at higher Bragg angles were obliterated. The (111) and (200) diffraction peaks characteristic of the fcc solid solution had only just begun to emerge. An additional 23 hours of milling eliminated the remaining elemental line at $2\theta = 68.7°$, and broadened the two fcc alloy peaks at $2\theta \approx 67°$ and $2\theta \approx 79°$; the (220) solid solution peak at $2\theta \approx 128°$ was now detectable. Milling for another 16 hours did not result in any appreciable change in the diffraction pattern. The diffractometer scan obtained on the powder milled for a total of 103 hours at a powder-to-ball ratio of 1:8.5 is shown in Figure 24, where its resemblance to the powder milled for 64 hours at a powder-to-ball ratio of 1:17 can be noted.

Annealing the powders milled for 103 hours at a powder-to-ball ratio of 1:8.5 resulted in both a sharpening and an increase in intensity of the fcc (111), (200) and (220) reflections, as expected (Figure 24c). To accomplish this, however, it was necessary to anneal the powders for longer times (or at higher temperatures) than were needed for the previous powder batch. This demonstrates that even after milling for 103 hours, the powders processed at the powder-to-ball ratio of 1:8.5 were not as homogeneous chemically as were the powders milled for only 64 hours at the 1:17 powder-to-ball ratio.

Microscopic examination of both batches of milled powders revealed significant differences in the particle size and particle morphology. The powder milled at the 1:17 powder-to-ball ratio exhibited plate-like morphology (Figures 25a and 25b). 72 w/o of the powder particles were larger than 74μm in diameter (Table IX). The powder milled at the higher powder-to-ball ratio (1:8.5) consisted almost entirely of coarse equiaxed particles (Figure 26); 95 w/o of the

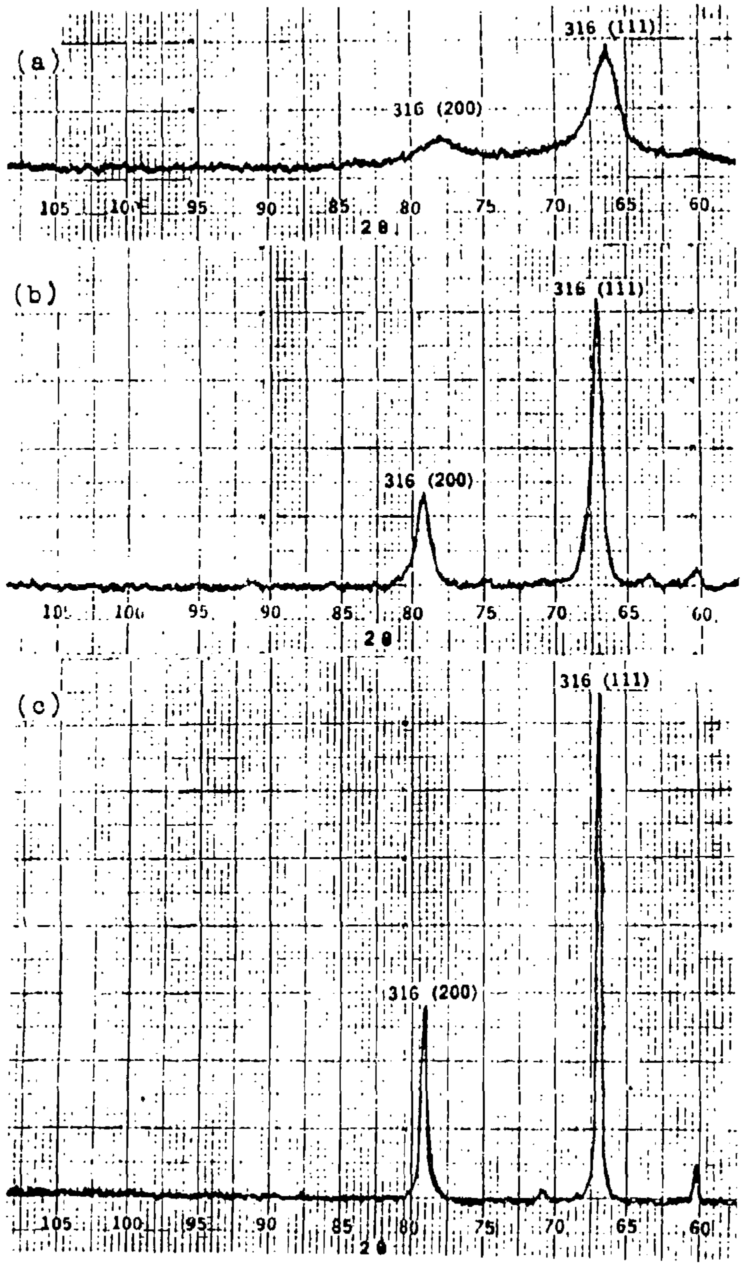

Figure 23 - X-ray diffraction spectra from 316 stainless steel powder mixtures (1:17 powder-to-ball ratio): a) milled for 64 hours at 300 RPM, b) same as (a), but annealed 1 hour at 650°C c) prealloyed type 316 stainless steel powder.

TABLE 7

PEAK INTENSITY AND PEAK BREADTH MEASUREMENTS
FOR AN OXIDE-FREE TYPE 316 STAINLESS STEEL POWDER MIXTURE MILLED AT 300 RPM
POWDER-TO-BALL RATIO = 1:17

MILLING TIME, HRS	ANNEALING TEMPERATURE AND TIME	α-Fe (110)*		316 (111)	
		RELATIVE INTENSITY I/I_o	FWHM 2θ, DEGREES	RELATIVE INTENSITY I/I_o	FWHM 2θ, DEGREES
0	—	1.0	0.4	0	—
16	AS-MILLED	0.15	1.2	0.23	1.5
32	AS-MILLED	0.04	1.4	0.24	1.5
48	AS-MILLED	—	—	0.24	1.5
64	AS MILLED	—	—	0.24	2.0
64	1 hr. at 500°C	—	—	0.25	1.6
64	1 hr. at 575°C	—	—	0.27	1.5
64	1 hr. at 650°C	—	—	0.56	0.75

*This peak corresponds to a superposition of the (110) reflections from α-Fe (bcc) and Cr (bcc), and the (111) reflection from Ni (fcc).

TABLE 8

EFFECT OF ANNEALING TEMPERATURE ON POSITIONS OF (111), (200), and (220) BRAGG PEAKS FOR MILLED 316 STAINLESS STEEL POWDER*

ANNEALING** TEMPERATURE, °C	(111) BRAGG ANGLE, 2θ	(111) 2θ, DEGREES	(200) BRAGG ANGLE, 2θ	(200) 2θ, DEGREES	(220) BRAGG ANGLE, 2θ	(220) 2θ, DEGREES
as-milled	63.3	—	78.0	—	126.5	—
500	66.7	0.4	78.5	0.5	127.0	0.5
575	66.8	0.5	78.7	0.7	128.5	2.0
650	67.1	0.8	79.2	1.2	129.2	2.7
Prealloyed 316 Stainless Steel Powder	66.9		79.2		128.7	

*Milled 64 hours at 300 RPM, 1:17 powder-to-ball ratio.

**Annealing time = 1 hr at all temperatures.

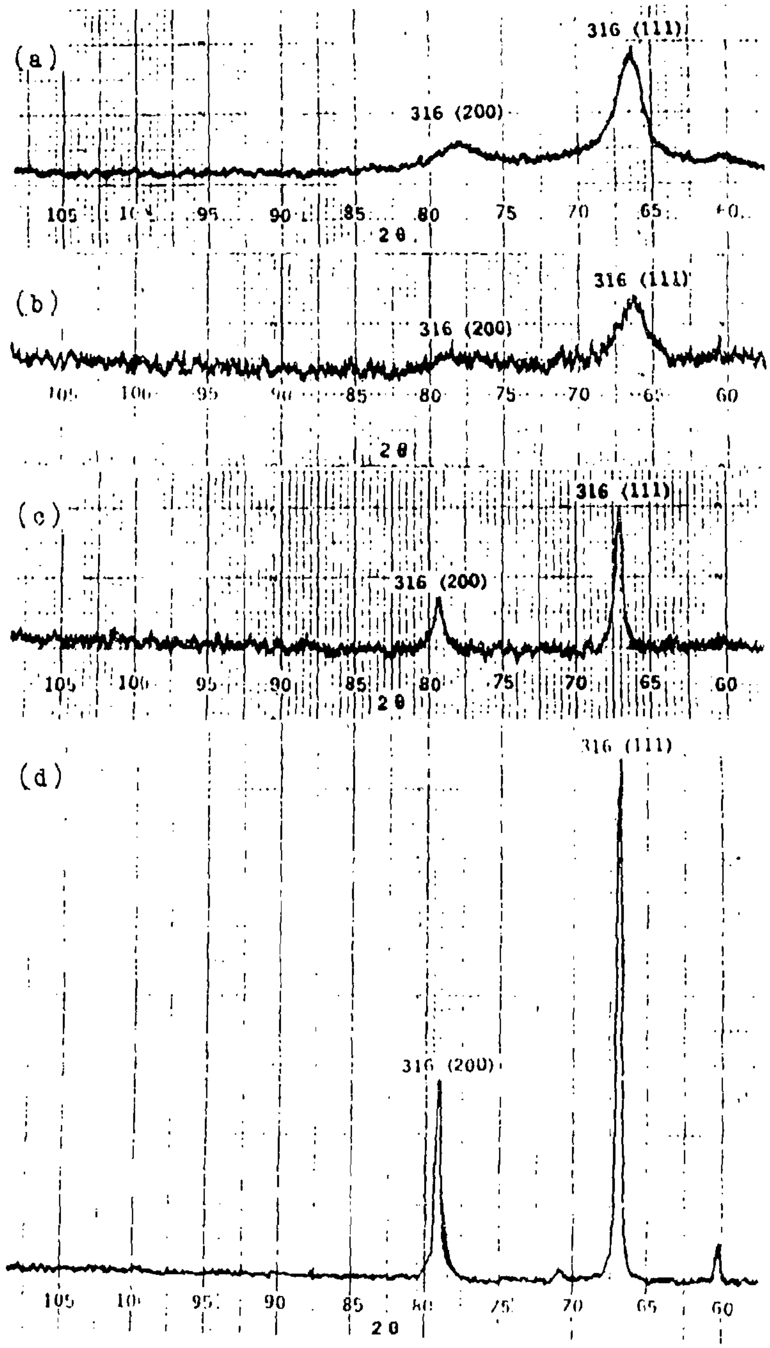

Figure 24 - X-ray diffraction spectra from 316 stainless steel powder mixtures: a) milled 64 hours at 300 RPM (1:17 powder-to-ball ratio), b) milled 103 hours at 300 RPM (1:85 powder-to-ball ratio), c) same as (b), but annealed for 3 hours at 700°C, d) prealloyed 316 stainless steel powder.

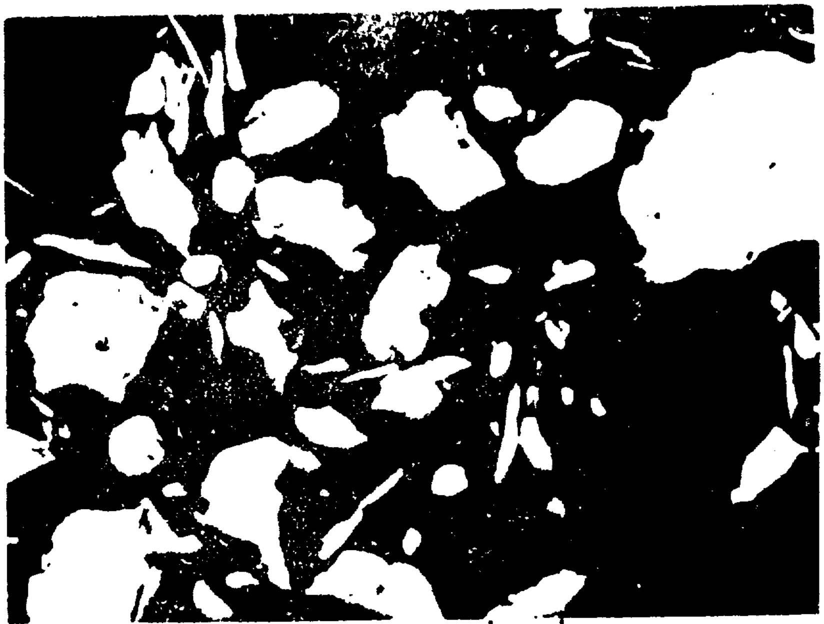

(a)

(b)

Figure 25 - 316 stainless steel powder mixture milled for 64 hours at 300 RPM; powder-to-ball-ratio = 1:17 a) optical micrograph, polished cross section, unetched, X200, b) SEM micrograph, X400.

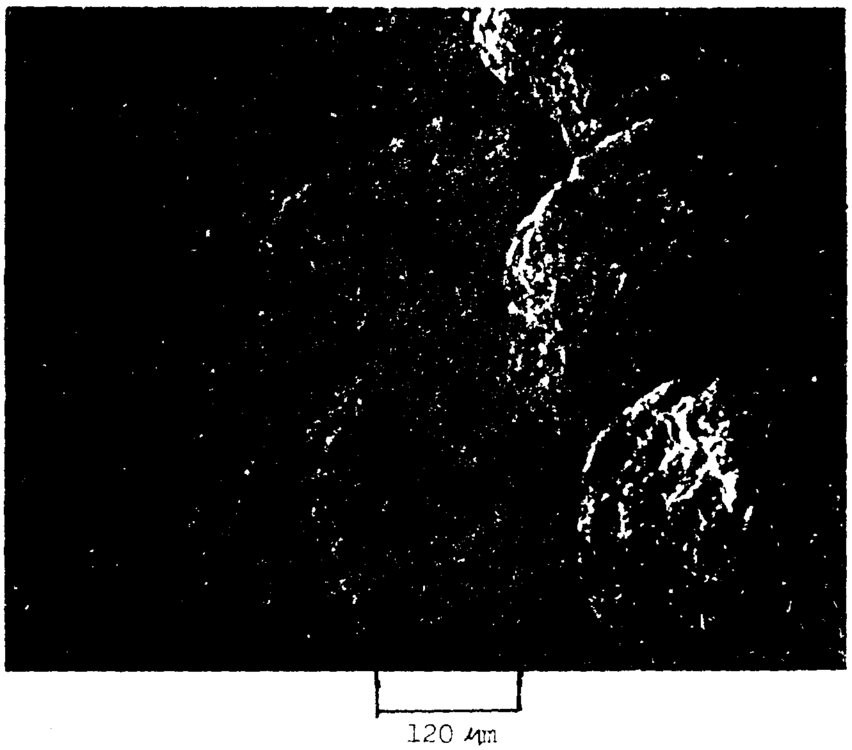

Figure 26 - SEM micrograph, 316 stainless steel powder mixture for 103 hours at 300 RPM: powder-to-ball ratio = 1:8.5. X170.

powder particles were greater than 177μm in diameter (Table IX). The quantity of fine powder (-44μm) was negligible in both systems.

The observed differences in particle shape or morphology can be correlated with the time required for the powder to discharge from the mill. At the 1:17 powder-to-ball ratio, more than eight hours were required for the powder to be completely discharged from the mill. Examination of the mill contents prior to discharge of the powder revealed that each individual ball was coated with metal powder; no free powder was present in the mill. Long times were apparently required to fracture the metal coating from each ball. This was responsible for the plate-shaped particles. In contrast, less than one hour was required for the powder to discharge from the mill at the 1:8.5 powder-to-ball ratio. The balls were coated with very little metal powder. Apparently, cold welding between the balls and the powder was negligible at the higher powder-to-ball ratio. This also accounts for the absence of plate-shaped particles in the powder distribution.

When metallographically polished samples of the powders milled for 64 hours (at a powder-to-ball ratio of 1:17) were etched in "super picral", it was found that the majority of the particles were passive to the etchant; those that did etch were not etched uniformly (Figure 27a), but exhibited striations, i.e., alternate light and dark etching bands. In contrast, after the powder was annealed for 1 hour at 650°C, the majority of the particles were uniformly attacked by the etchant (Figure 27b). This might also be taken as an indication that the milled stainless steel powder was not chemically homogeneous to begin with, although the interpretation is complicated by the fact that the milled powders are also heavily cold-worked.

Note that the as-milled powder was magnetic whereas the annealed powder was not. Before the powders were annealed, therefore, unprocessed iron fragments (or iron-rich bcc solid solutions) must have been present even though elemental Bragg reflections could not be detected in the X-ray diffractometer scans. Enough homogenization obviously occurred during annealing to eliminate structural and compositional inhomogeneities of this kind. The fact that distinct shifts in the positions of the Bragg peaks were also observed on annealing, along with changes in the magnetic behavior and in etching response, definitely establishes that the milled powders were neither chemically nor structurally homogeneous on a scale of atomic dimensions.

7-2b. Effect of TiO Additions

Additions of TiO_2 to the elemental Type 316 stainless steel powder mixture increased, by at least a factor of four, the time required for an equivalent degree of processing under otherwise identical milling conditions. This effect appeared to be roughly independent of the amount of TiO_2 added in the range from 1-3 w/o TiO_2. 900 gram changes containing various quantities of the oxide were milled at 300 RPM at a powder-to-ball ratio of 1:17. Peak intensity measurements on a representative powder charge containing 2.5 w/o TiO_2 are summarized in Table X.

TABLE 9

SCREENED PARTICLE SIZE ANALYSES OF MECHANICALLY ALLOYED
OXIDE-FREE 316 STAINLESS STEEL POWDERS

MESH SIZE	PARTICLE SIZE RANGE, μm	PERCENTAGE BY WEIGHT POWDER-TO-BALL RATIO=1:17 64 HRS AT 300 RPM	POWDER-TO-BALL RATIO=1:8.5 103 HRS AT 300 RPM
+40	+420	0	43
-40, +80	-420, +177	28	52
-80, +200	-177, +74	44	2
-200, +325	-74, -44	26	1
-325	-44	2	2

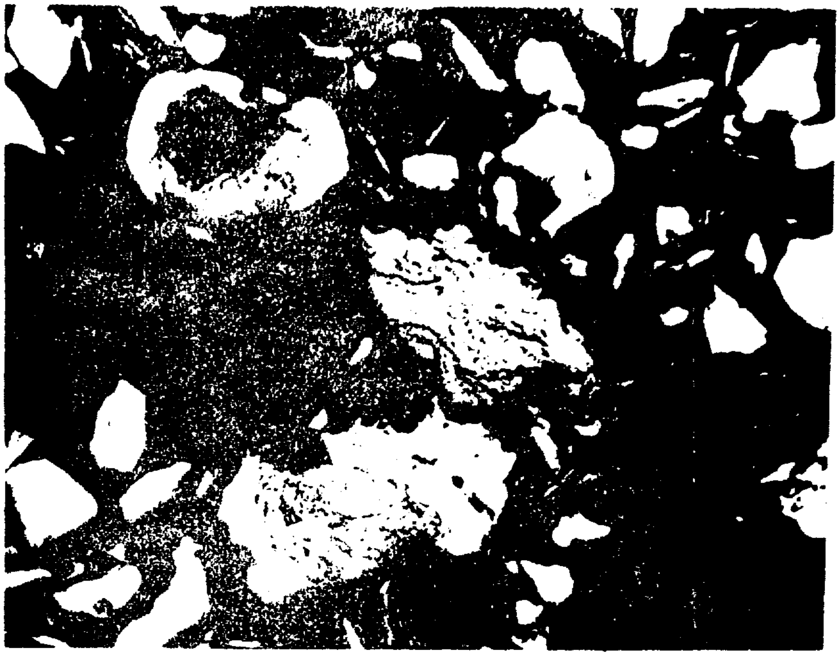

(a)

(b)

50 µm

Figure 27 - Polished and etched cross sections of 316 stainless steel powder mixture milled 64 hours at 400 RPM: powder-to-ball ratio - 1:17. a) as-milled, super picral etch. X200, b) annealed 1 hour at [illegible]°C. super picral etch, X[illegible].

TABLE 10

PEAK INTENSITY MEASUREMENTS
316-2.5 w/o TiO_2 POWER MILLED 98 HOURS AT 300 RPM
POWDER-TO-BALL RATIO = 1:17

MILLING TIME, HRS	RELATIVE INTENSITY, I/I_o α-Fe (110)	316 (111)
0	1.0	0.0
6	0.38	0.0
23	0.20	0.0
30	0.19	0.0
47	0.16	0.0
54	0.15	0.0
71	0.12	0.15
92	0.0	0.25

After milling for 6 hours the most intense Bragg peak from TiO_2 (i.e., the (101) reflection at $2\theta=38^\circ$), along with most of the lower intensity elemental peaks were obliterated. Further milling resulted in the continuous broadening and reduction in intensity of the remaining elemental Bragg peaks. After 70 hours, the (111) and (200) Bragg reflections corresponding to the fcc solid solution began to emerge; however, the elemental α-Fe (110) peak at $2\theta=68.7^\circ$ was still present. The extent of processing achieved at this stage was about equivalent to that obtained in only 16 hours with oxide-free powders. After 92 hours of milling, the elemental α-Fe (110) peak had disappeared and the (220) Bragg peak for the fcc solid solution was now detectable in the diffractometer scan.

Although the amount of TiO_2 added is not an important variable insofar as the rate of processing is concerned, the particle morphology is significantly affected by the quantity of oxide present. High-energy milled powders containing 1 w/o TiO_2 had a pronounced plate-like morphology identical to that of the oxide-free powder shown in Figures 25a and 25b. The plate-shaped particle morphology is attributable to the welding of the powder to surfaces of the balls. The majority of the powder particles consist of fragments that had fractured from the ball surfaces during the long times required for discharge from the mill. Powders containing only 1 w/o TiO_2 did not behave much differently, in this respect, than the oxide-free powders.

Increasingly larger quantities of oxide resulted in powder particles having more nearly spherical shape. Thus, the particles from the batches containing 2, 2.5 and 3 w/o TiO_2 were basically equiaxed, as shown in Figure 28. When 2 w/o or more of TiO_2 was present, the metal powders did not exhibit as strong a tendency to cold weld to the ball surfaces as did the oxide-free powder or the powder containing only 1 w/o TiO_2. Discharge times were short since fracturing of the powder from the ball surfaces was not required. The nearly equiaxed particle morphology is therefore understandable.

It was found that the size distribution of the powder particles was also significantly influenced by the amount of TiO_2 present. This is illustrated by the screened particle size analyses summarized in Table 11, in which it can be seen that increasing oxide additions tend to produce powder particles of finer particle size.

To evaluate the uniformity of the oxide distribution, powders containing 2.5 w/o TiO_2 were annealed at increasingly higher temperatures in range from 500°C to 1100°C. This was done in order to deliberately coarsen the distribution so that the TiO_2 particles could then be resolved metallographically. Microhardness measurements and X-ray diffractometer scans were also carried out on the annealed powders in addition to metallographic observations. The microhardness measurements are presented in Table 12, along with data on the relative intensity of the (111) Bragg reflection. It may be observed that the hardness first increases and then falls continuously as the annealing temperature is raised (resulting from oxide particle coarsening) while the relative intensity of the (111) Bragg peak increases monotonically.

Only after the powders were annealed for 1.5 hours at 1100°C could the oxide particles be resolved metallographically. The resulting oxide distribution is

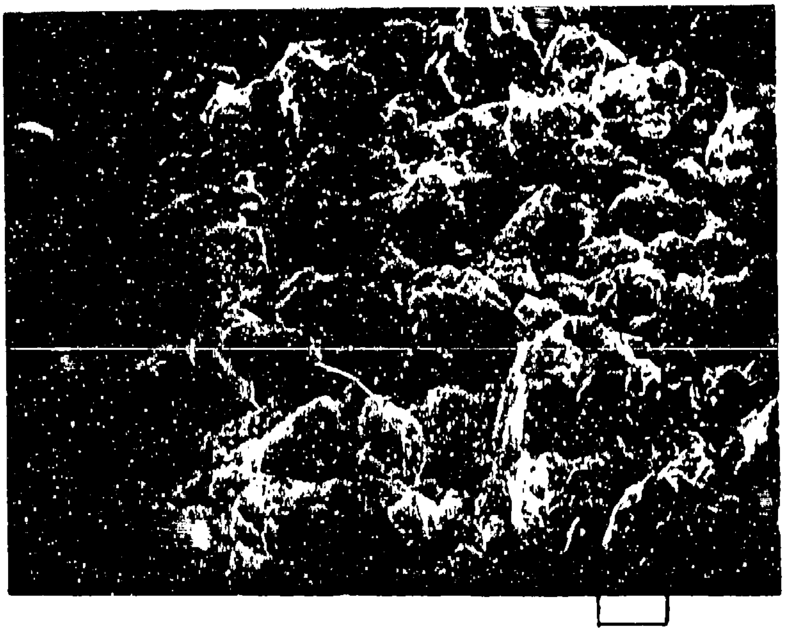

Figure 28 - SEM micrograph 316-3 w/o TiO_2 powder milled 96 hours at 300 RPM, X1000.

TABLE 11

SCREENED PARTICLE SIZE ANALYSES
316 STAINLESS SYSTEM
POWDER-TO-BALL RATIO=1:17, MILLED AT 300 RPM

		PERCENTAGE BY WEIGHT				
MESH SIZE	PARTICLE SIZE, m	0 w/o TiO_2 MILLED 64 HOURS	1 w/o TiO_2 MILLED 96 HOURS	2 w/o TiO_2 MILLED 93 HOURS	2.5 w/o TiO_2 MILLED 98 HOURS	3 w/o TiO_2 MILLED 92 HOURS
-40, +80	-420, +177	28	23	46	1	0
-80, +100	-177, +74	44	13	50	49	15
-200, +325	-74, +44	26	36	4	35	61
-325	-44	2	28	0	15	24

TABLE 12

EFFECT OF ANNEALING TEMPERATURE ON PARTICLE HARDNESS
AND RELATIVE INTENSITY OF THE (111) BRAGG REFLECTION
316 STAINLESS STEEL - 2.5 w/o TiO_2 POWDER
98 HOURS AT 300 RPM*

ANNEALING TEMPERATURE, °C*	RELATIVE INTENSITY, I/I_0	AVG KHN
As-Milled	0.13	780
500	0.15	935
600	0.18	870
700	0.30	825
800	0.35	702
900	0.47	635
1000	0.61	528
1100	0.66	418
Prealloyed 316 SS	1.0	126

*Annealing time = 1.5 hours at all temperatures.

shown in Figure 29. Since the oxide distribution after coarsening is quite uniform, it may be concluded that the initial oxide distribution must also have been relatively uniform.

A similar experiment was undertaken to determine the uniformity of the oxide distribution in high-energy milled Fe - 10 w/o TiO_2 powders. The powder was milled for 64 hours at 300 RPM (1:17 powder-to-ball ratio), cold pressed at 70 ksi and then sintered for 2 hours at 1300°C in argon to coarsen the oxide distribution. Metallographic examination of the sintered samples showed distribution of oxide particles was remarkably uniform (Figure 30a) after coarsening. The coarse oxide particles were also clearly evident via scanning electron microscopy (Figure 30b). Thus, even when much larger quantities of oxide are present (in this case 10 w/o), the oxide particles appear to be dispersed on a uniform scale by high-energy milling.

-2c. Cold Compaction Behavior of Mechanically Alloyed 316 Stainless Steel Powders

Sound green compacts could not be prepared from either the oxide-free or the oxide-dispersed 316 stainless steel powders in the "as-milled" (cold-worked) condition. Ejection of the samples from the die after compaction at 80 or 100 ksi resulted in catastrophic separation of the compacts, i.e., in delaminations within the samples. This behavior can be attributed to elastic recovery of the compact. When the pressure is released from the powder by removing the punches, axial expansion within the compact occurs. The degree of expansion depends on the magnitude of the original elastic strains and the degree of mechanical interlocking between the particles (which acts to restrain elastic recovery). The lower the elastic modulus and the higher the yield strength of the materials, the greater the amount of elastic deformation and hence the greater the elastic recovery. The delamination behavior of the compacts is further aggravated when the compact is ejected from the die cavity. Radial expansion may now cause cracks to propagate and link up to form the large scale fissures. During compaction of the cold-worked, milled powders, insufficient plastic deformation, and thus negligible mechanical interlocking occurred. This led to delamination of the green compacts upon ejection from the die.

Similarly, the compaction behavior of oxide-dispersed powders was not significantly improved by annealing for 1 hour at 650°C prior to compaction; i.e., low density, delaminated samples still resulted upon ejection from the die. This can be seen in Figure 31a in which the cross-sectional area of 316 - 3 w/o TiO_2 green compact pressed at 80 ksi is shown. The green density was measured to be 5.1 gm/cm^3 corresponding to 65% theoretical density. Compaction of the oxide-dispersed powders at 100 ksi resulted in a slightly higher green density, but delaminations were still present. In contrast, catastropic separation of the oxide-free 316 compacts was not experienced after the powder was annealed. Shown in Figure 31b is the cross-sectional area of the oxide-free green compact, also compressed at 80 ksi. Higher green density, sound green compacts were obtained with the annealed oxide-free powders. This can be attributed, in part, to the softer, non-dispersion strengthened particles (which permits more plastic deformation during compaction), but also to the fact that the particles are of non-spherical

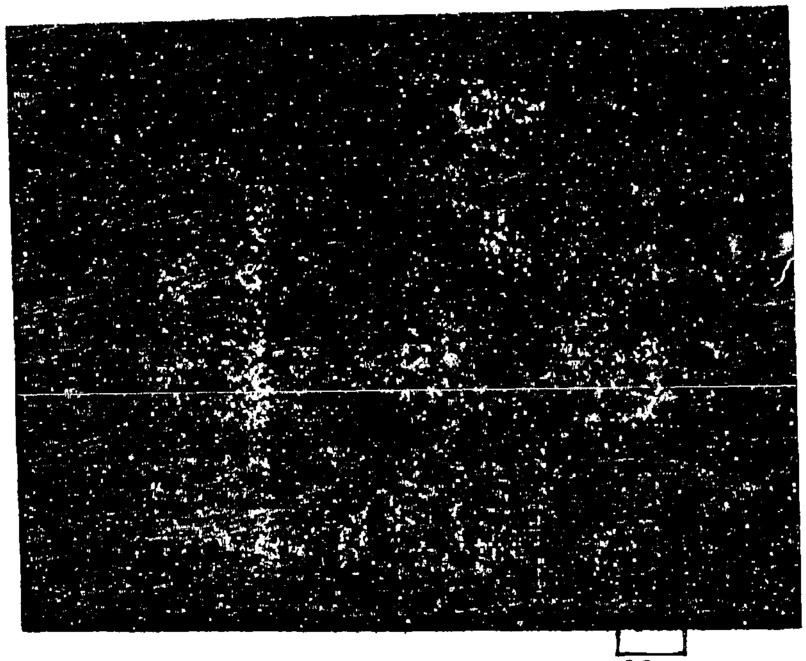

Figure 29 - Optical micrograph, 316-2.5 w/o TiO_2 milled 98 hours at 300 RPM. Annealed 1.5 hours at 1100°C, X750; unetched.

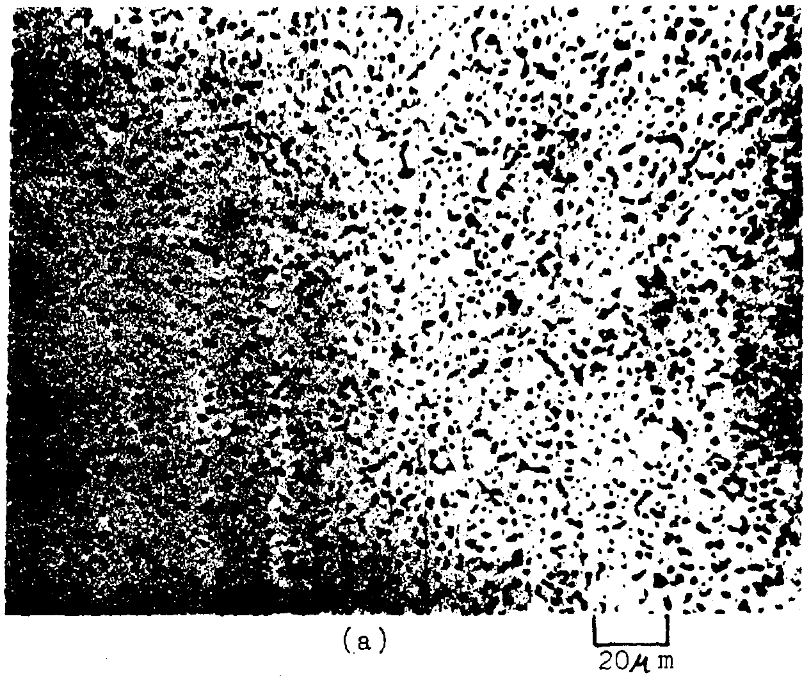

(a)

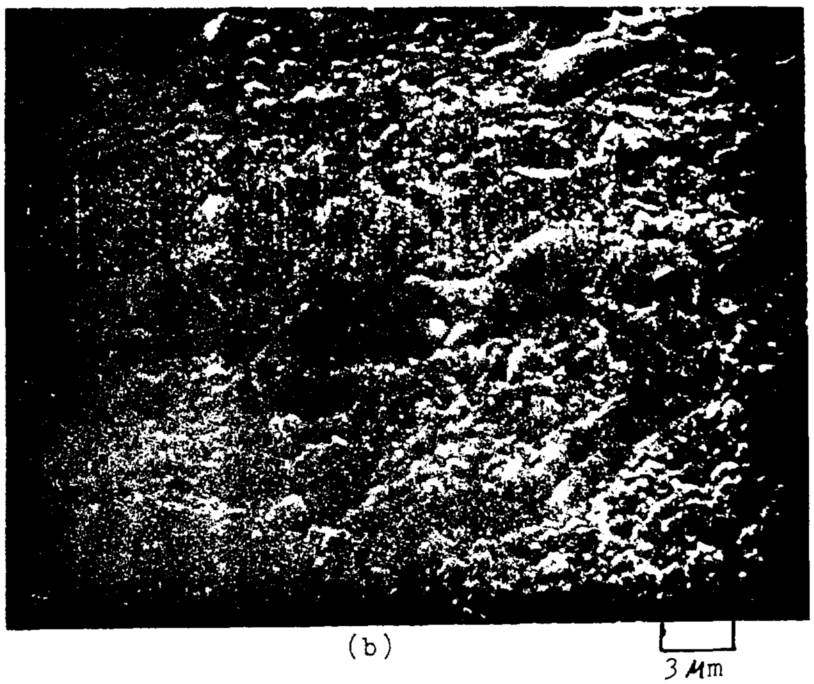

(b)

Figure 30 - Iron -10 w/o TiO_2 powder milled 64 hours at 300 RPM, compacted at room temperature to 70 KSI, and annealed for 2 hours at 1300°C a) polished and unetched cross section, X500, b) SEM micrograph, nital etch, X3800. Note the TiO_2 rich phase.

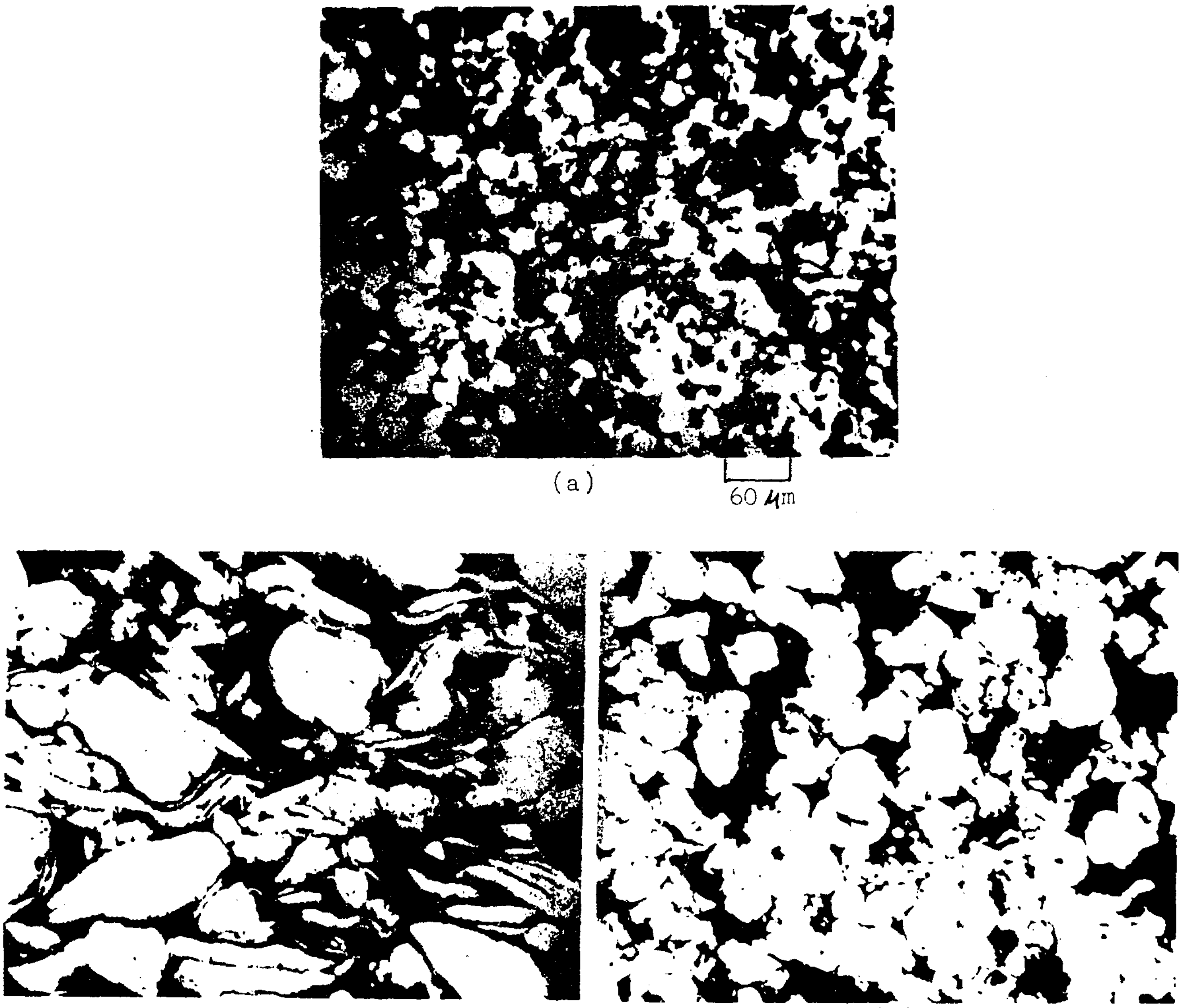

Figure 31 - Optical micrographs of powders; 160X, a) 316-3 w/o TiO_2 powder milled 2 hours at 300 RPM, annealed 1 hour at 650°C, compacted at room temperature to 80 KSI, b) oxide-free 316 powder milled 64 hours at 300 RPM, annealed 1 hour at 650°C, and compacted at room temperature to 80 KSI, c) atomized, prealloyed 316 powder compacted at room temperature to 80 KSI

particle shape. The oxide-dispersed powders, on the other hand, have nearly spherical shapes which results in only point contact between adjacent particles when they are pressed. Even with significant amounts of plastic deformation, sufficient green strength to hold the particles together does not develop. Consequently, even though densification occurs during compaction, ejection from the die results in compacts having low green density, and also leads to delamination within the compact.

The compaction behavior of the high-energy milled powders is quite different from that of the atomized, prealloyed 316 stainless steel powder. Compaction of the prealloyed powders (of spherical shape) at 80 ksi (Figure 31c) resulted in green densities of approximately 6.3 gm/cm^3 (80% theoretical density); no delaminations within the compacts were produced upon ejection from the die. The extremely soft condition of the atomized powder permitted large amounts of plastic deformation to occur and therefore made it possible to obtain substaintially higher green densities and green strengths despite the spherical particle shape.

7-3 THE β-Ti SYSTEM (MODIFIED Ti-13v-11Cr-3A1)

Milling difficulties, similar to those observed by Wright and Clauer[13], were encountered in the processing of the β-Ti alloy powders which precluded any conclusions pertaining to the chemical or structural homogeneity of the milled powders. After 64 hours of milling at 300 RPM (1:17 powder-to-ball ratio), the powder could not be discharged from the mill. It was found that the original powder charge had welded into one large mass which had attached itself to the bottom of the mill container (Figure 32a). This welded material consisted of an agglomerate of extremely fine (sub-micron size) powder particles of roughly equiaxed shape (Figure 32b). An x-ray diffraction analysis of this material did not reveal the presence of any elemental or alloy diffraction peaks.*

As previously mentioned, Wright and Clauer experienced similar difficulties in milling oxide-dispersed Ti-Al alloys[13]. They concluded the agglomeration of powders had resulted from the heating up of the charge during prolonged processing to a point where diffusion bonding of the individual particles had occurred. This conclusion seems quite likely for the β-Ti system also since weld deposits originated in β-Ti system after 20 hours of uninterrupted milling, but were not detected prior to 20 hours of milling. However, it is suspected the behavior of the β-Ti system is also related to the hexagonal close-packed crystal structure of the titanium, and its associated smaller strain hardening rate (compare to the other cubic crystal structures). Note that welded deposits were not characteristic of the previous systems investigated; i.e., the bcc Cr-Mo and the fcc 316 stainless steel.

---

*The fact that no diffraction peaks were present in the diffraction scans for the β-Ti system is not totally surprising considering that titanium has a very large mass absorption coefficient (603 cm^2/gm) for soft (long wavelength) X-rays. Thus, the CrK_α radiation (λ =2.291Å) was easily absorbed by titanium. As for the diffraction peaks corresponding to the other elements in the powder system, they were probably severely broadened to such a degree so as to avoid detection.

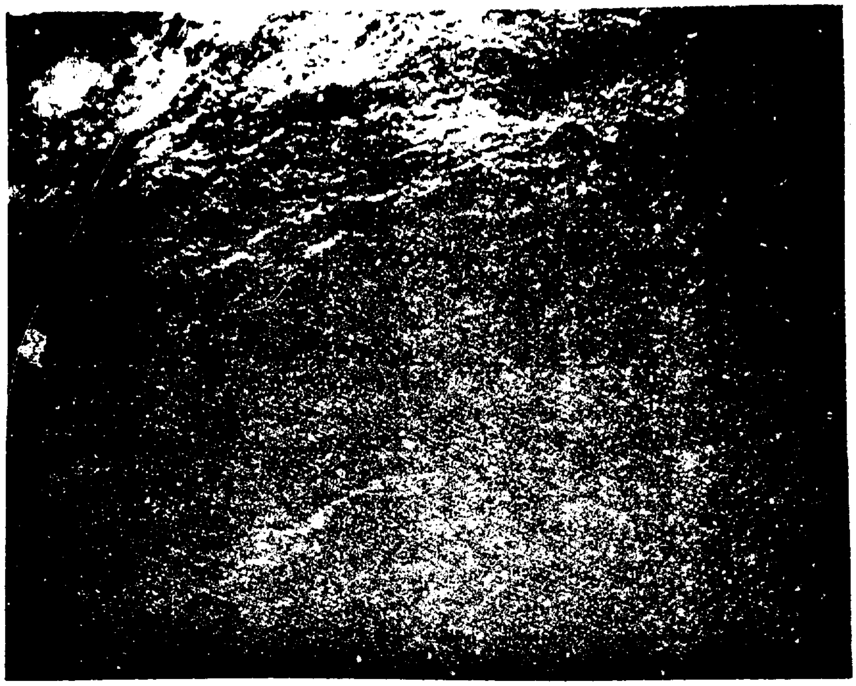

(a)

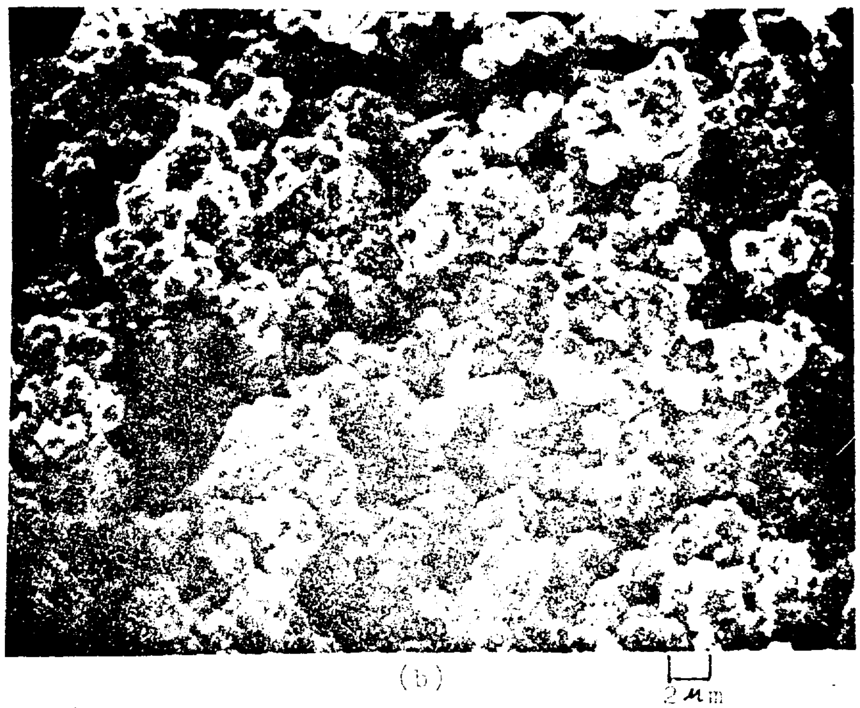

(b)

Figure 32 - SEM micrographs of the modified Ti-13V-11Cr-3Al elemental powder mixture which had welded onto the bottom of the mill container after milling for 64 hours at 300 RPM. a) 60X. b) 3100X.

For systems of this type, which exhibit a pronounced tendency to cold weld and/or diffusion bond and a small strain hardening rate, it appears as though it is not possible, without additional processing parameters, to achieve the proper balance between cold welding and fracturing to mechanically alloy the component metals. Steps to either decrease the tendency for cold welding or increase the work hardening rate of the particles must be insured for any possible success of the mechanical alloying process. One such step is milling in a liquid nitrogen atmosphere to reduce the processing temperature, such as Nix and White[16] did. For their particular system, Nb_3Sn, room temperature represented a warm working temperature (where one would also expect the tendency to cold-weld or diffusion bond to be dominate) and milling in a continuous stream of liquid nitrogen was necessary to disperse the Nb and Sn powders.

7-4 THE BISMUTH-MANAGANESE SYSTEM

Milling difficulties identical to those observed in the β-Ti system were also encountered with bismuth-manganese powder mixtures which prevented mechanical alloying of the component metals. After only 16 hours of milling at 300 RPM (1:16 powder-to-ball ratio), the powder would not discharge from the mill. An X-ray diffraction analysis of the material that had welded onto the bottom of the container revealed only the presence of broadened elemental peaks from both bismuth and manganese.

Ball milling another batch of the bismuth-manganese powder mixture, at a lower mill speed of 150 RPM (1:16 powder-to-ball ratio), did not alter the results; the powder had still welded onto the bottom of the mill. Milling speeds less than 150 RPM were not investigated.

As such, the attempts to produce the MnBi (NiAs structure) via high energy milling were unsuccessful. In contrast, a MnBi intermetallic phase powder has been prepared by ball milling in a conventional ball mill, then annealing at temperatures just below the melting point of elemental bismuth[24]. What one can now infer in mechanical alloying of MnBi is that perhaps too much energy is transmitted to the component metals via high energy milling. This apparently increased the processing temperature to a point where, as in the β-Ti system, the tendency for the particles to diffusion bond was dominate, and thus the tendency for particle fracturing had been reduced. As a result, mechanical alloying cannot take place.

7-5 SLURRY MILLING

Slurry milling was tried in an effort to process powder systems that behave in a fashion similar to Bi-Mn and β-Ti in which the tendency to diffusion bond is dominate. In such systems, the proper balance between cold-welding and fracturing cannot be obtained by dry powder processing unless the processing temperature is reduced; heating promotes diffusion bonding and the tendency to weld far exceeds the rate of particle fracturing in both these systems. It was hoped slurry milling would reduce, but not completely eliminate cold welding. Unfortunately, attempts to produce a 316 alloy powder by slurry milling in liquid mediums of benzene or isopropanol, were unsuccessful. Alloy powders could not be prepared regardless of the milling time employed, and the resulting powders were also pyrophoric.

It appears that when metal powders are processed in liquid mediums there is a total absence of cold welding; only particle fracturing results. This became apparent during the SEM and X-ray analysis of the powders that were slurry milled for 120 hours. The diffraction spectra from this powder only exhibited elemental peaks; diffraction peaks corresponding to the 316 alloy were not present. Yet, the particles were measured to be approximately 0.1μm diameter in size. This is over two orders of magnitude smaller than particles that result from dry powder processing. Furthermore, it was noted that the resulting particle morphology is identical to that of the powders in the powder system prior to slurry milling. That is, slurry milling of particles initially plate-shaped resulted in particles approaching the sub-micron range, but still retaining the plate-like shape (Figure 33), and slurry milling of particles with spherical morphology resulted in sub-micron particles with equiaxed morphology. Regardless of the particle shape, metal powders produced by slurry milling having particle sizes in the sub-micron range are pyrophoric.

Figure 33 - SEM micrograph of oxide-free 316 stainless steel powder prepared by mechanical alloying (64 hours at 300 RPM in argon). Subsequently the powder was slurry milled 20 hours in isopropanol at 225 RPM. X2300.

8. SUMMARY AND CONCLUSIONS

The following conclusions concerning the mechanical alloying process can be drawn from this investigation:

1. It was established that in both the Cr-Mo and Type 316 stainless steel system, elemental components had become interdispersed on an atomic scale during milling, but the resulting solid solutions are structurally, as well as chemically, inhomogeneous.

2. In both the Bi-Mn and β-Ti systems, the tendency toward cold welding and/or diffusion bonding of the particles was so pronounced that it was not possible to achieve a proper balance of cold-welding and particle fracturing in order to mechanically alloy component metals; the powder tends to weld into one large mass onto the bottom of the milling container. Additional processing steps, e.g., milling in a liquid nitrogen atmosphere, are required to insure mechanical alloying.

3. TiO_2 additions to the 316 stainless steel system retarded the rate of processing by a factor of four.

4. The quantity of TiO_2 oxide present in the 316 stainless steel system produced significant changes in the particle size, size distribution, and morphology.

5. A uniform oxide distribution within the 316 powder particles resulted by mechanical alloying.

6. An increase in the powder-to-ball ratio from 1:17 to 1:8.5 retarded the alloying rate by a factor of four in 316 stainless steel system.

7. An increase in the milling speed by a factor of two (from 150 RPM to 300 RPM) has been shown to increase the rate of processing by over an order of magnitude in the Cr-Mo system.

8. During slurry milling, there is a total absence of cold welding. Only particle fracturing results which can lead to the production of sub-micron particles which are pyrophoric.

REFERENCES

1) Benjamin, J.S., Met. Trans., 1, 2949 (1970)

2) Benjamin, J.S., Scientific American, 234(5), 40 (1976)

3) Benjamin, J.S., U.S. Patent No. 3,728,088, (April 17, 1973)

4) Grant, N.J., "Dispersed Phase Strengthening", The Strengthening of Metals, ed. by D. Peckner (New York, Rhenhold Publishing Corp.), (1967), P.163

5) Irmann, R., Metallurgia, 46, 125 (1952)

6) Murphy, R., and Grant, N.J., Powder Met., 10, (1962)

7) Smith, C.S., Mining and Metallurgy, 11, 213 (1930)

8) Himmel, L., and Mitchell, J.B., Proceedings, Second International Conference on the Strength of Metals and Alloys, Vol II, 654 (1970)

9) Bonis, L.J. and Grant, N.J., Trans. Met. Society AIME, 224, 308 (1962)

10) Preston, O., and Grant, N.J., Trans. Met. Society AIME, 221, 164 (1961)

11) Merrick, H.F., Curwick, L.K. Kim, Y.G., "Development of an Oxide Dispersion Strengthened Turbine Blade Alloy by Mechanical Alloying", NASA Report No. CR-135150, (1977)

12) Benjamin, J.S., "Oxide Dispersion Strengthened Superalloys for Advanced Gas Turbines", Technical Paper 915T-OP, Presented at 21st Int. Gas Turbine Conference, (1976)

13) Wright, I.G., and Clauer, A.H., "Study of Intermetallic Compounds TASK A: Dispersion Hardened TiAl", Technical Report AFML-TR-76-107, (1976)

14) Stringer, J., Wilcox, V.A. Jaffee, R.I., Oxidation of Metals, 5(1), 11 (1972)

15) Stringer, J., Wright, I.G., Oxidation of Metals, 5(1), 59 (1972)

16) White, R.L., and Nix, W., "Application of Mechanical Alloying to the Manufacture of Cu-Nb_3Sn Multifilimentary Superconducting Wire", New Developments and Applications in Components, ed. by K. Kulhmann - Wilsdorf and W.C. Harrigon, Jr., Conference Proceedings - Met. Soc. of AIME, (1978)

17) Larson, J.M., Luhman, T.S., and Merrick, H.F., Proc. of Intern Conf. on Manufacture of Superconducting Materials, ASM (1976) p.155

18) Benjamin, J.S. and Volin, T.E., Met. Trans., 5, 1927 (1974)

19) Glaskow, T.K., "An Oxide Dispersion Strengthened Alloy for Gas Turbine B sdes", NASA Technical Memorandum 79088 (1979)

20) Pearson, W.B., Lattice Spacing and Structures of Metal and Alloys, (New York, Pergamon Press), 548 (1958)

21) ASM Metals Handbook, Vol. 8 (1973) P.291

22) Hultgren, R., DeSai, P., Hawkins, D.T., Gleiser, M., and Kelly, K.K., Selected Values of Thermodynamic Properties of Binary Alloys, ASM, (1973)

23) Wood, R.A., Favor, R.J., Titanium Alloys Handbook, Metals and Ceramic Information Center, MCIC-H8-02 (1972) P. 1-9:72-1

24) Cornish, A.J., U.S. Patent 2,865,085, (Dec 23, 1958)

25) Askill, J.S., "Tracer-Diffusion Studies in Molybdenum," Diffusion in Body Centered Cubic Metals, ASM, (1965) p.247

26) Askill, J.S. "Self Diffusion in Chromium", Diffusion in Body Centered Cubic Metals, ASM, (1965), p.253

DISTRIBUTION LIST

	Copies
Defense Documentation Center ATTN: TIPDR Cameron Station Alexandria, VA 22314	12
Director US Army Materials and Mechanics Research Center ATTN: DRXMR-M Watertown, MA 02172	2
Commander US Army TACOM ATTN: DRSTA-UL (Technical Library) Warren, MI 48090	2
Commander Air Force Materials Laboratory ATTN: LTM Wright-Patterson AFB, OH 45433	1
NASA - LERC Technical Library 21000 Brook Park Rd. Cleveland, OH 44135	1